N70-11779
TMX-63738

X-551-69-403
PREPRINT

CASE FILE
COPY

IONOSPHERIC PERTURBATIONS ON STADAN VHF TRACKING ACCURACY

B. ROSENBAUM

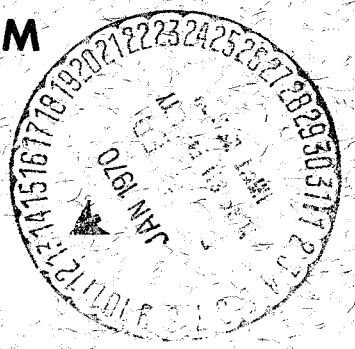

SEPTEMBER 1969

GSFC
GODDARD SPACE FLIGHT CENTER
GREENBELT, MARYLAND

X-551-69-403
PREPRINT

IONOSPHERIC PERTURBATIONS ON STADAN VHF TRACKING ACCURACY

B. ROSENBAUM

September 1969

GODDARD SPACE FLIGHT CENTER
Greenbelt, Maryland

X-551-69-403

IONOSPHERIC PERTURBATIONS ON STADAN VHF TRACKING ACCURACY

by

B. Rosenbaum

ABSTRACT AND SUMMARY

Ionospheric propagation effects are a major factor limiting tracking accuracy of the VHF systems of STADAN (Satellite Tracking and Data Acquisition Network). These systems are comprised of Minitrack which is an interferometer scheme for precision measurement of direction cosines and the VHF Goddard Range and Range-Rate (GRARR) system which measures range, range-rate, and angle. The extent of ionospheric perturbations is large or small depending on the state of the ionospheric medium and the mode and circumstance of the tracking operation. Under conditions of maximum total integrated electron content ($N_t \doteq 10^{18}$ e/m^2) the perturbation in GRARR can amount to about 5 km in range and 20 meters/sec in range-rate. These numbers exceed instrumental tracking precision by more than two orders of magnitude. In Minitrack, the ionospheric perturbations can exceed instrumental precision by a factor of 20. The complex behavior of the ionosphere makes these perturbations difficult to predict in

sufficient detail for the needs of precise tracking. A consequence is the introduction of a relatively large element of uncertainty into system and mission analysis. This applies in particular to evaluating the effectiveness of the currently employed STADAN ionospheric correction model. The approach of this paper to these problems is first to give a parametric analysis of the ionospheric perturbations. A special concern in the study is to establish the significance of the horizontal gradients within the ionospheric medium. In this regard, journal publications are surveyed for observational data pertaining to the level of horizontal gradients of N_t. The interest for Minitrack is that a finite refraction prevails at the zenith which, at times, can exceed instrumental errors. A general result emerging from the analysis of ionospheric perturbations is the central role of N_t and its horizontal gradients. The limitation to correction of ionospheric effects on tracking data stems from the wide variability and irregular temporal behavior of N_t as well as its geographical dependence. An observational scheme is sketched for the monitoring of N_t at STADAN sites which could materially relieve the limitation.

IONOSPHERIC PERTURBATIONS ON STADAN VHF TRACKING ACCURACY

I. INTRODUCTION

The ionosphere exerts a degrading effect on the tracking accuracy of the STADAN VHF systems. These perturbations, characteristically, are highly variable depending on the state of the ionosphere and on the mode and circumstance of the tracking. Accordingly, the ionosphere can be a dominant factor in limiting system accuracy or have only a minimal effect. In an overall systems view there prevails, due to ionospheric influence, a considerable disparity between instrumental design precision and the tracking accuracy. Nonetheless, the STADAN systems have a long achievement record for the tracking support of scientific satellites. The STADAN hardware performance is well established both in basic analytic studies and in field tests. The recent design evaluation report on the Goddard Range and Range Rate system (GRARR) gives a detailed analysis on instrumental metric accuracies (Ref. 1). In the GEOS-I project notable contributions are made toward the improvement and verification of STADAN tracking accuracy. Among the several intercomparison system studies of this project, the accuracy of Minitrack has been demonstrated to approach that of the instrumental design (Ref. 2). The STADAN station positions have in addition been determined with increased certainty through the geodetic tie-in with the Smithsonian Astrophysical Observatory Standard Earth C-5 model

(Ref. 3). These accomplishments would in themselves appear to confer on the VHF GRARR system and on Minitrack the status of a precision tracking system. Yet this is denied or at least compromised by ionospheric propagation effects (Refs. 4 and 5).

A correction procedure for ionospheric and tropospheric refraction is used in STADAN (Ref. 6). The model is based on the ionospheric data published by ESSA in Ionospheric Predictions. Some improvement in tracking data is possible, thereby, provided the data corresponds to a period during which the ionosphere is, in the mean, adequately represented by the predictions. But this is an over-simplified view of ionospheric behavior since the medium undergoes wide and irregular variations. One can expect that the corrections of VHF range measurements in particular will suffer from the gross character of the ionospheric data and that a large bias may prevail. An underlying shortcoming is the lack of a direct observational method on the ionosphere to validate the data.

In the precise calculation of Minitrack orbits, data is confined to tracking at small zenith angles (less than 20°). This restriction is imposed to minimize refraction despite a program of ionospheric correction. One finds furthermore in reports a general prevailing uncertainty in the analysis of refraction effects (Ref. 7).

Although the ionosphere is a major limiting factor in VHF tracking accuracy the problem has not received adequate treatment. There is a notable imbalance

of effort to the detriment of the ionospheric factor. This deficiency should be rectified. There is a need for parametric analysis of the ionospheric effects on tracking accuracy and a need dictated by goals of tracking system performance for appropriate modeling of the ionospheric medium. We furthermore want to understand perturbations as a factor in system problems. To lend clafification and provide a background for these matters we endeavor now to sketch the ionospheric-tracking interrelation in several of its varied aspects.

The bearing of ionospheric perturbations on tracking system performance is linked with characteristic detailed behavior of ionospheric structure. Certainly the most distressing feature of tracking errors having an ionospheric origin is the large magnitude of the errors and their irregular changes. Ionospheric patterns are noted for their variability and their unpredictability. A basic parameter for the measure of ionospheric perturbation on tracking is, N_t, the total integrated electron content within a vertical column of unit cross-section extending through the ionospheric layer. An example illustrating the diurnal variability of N_t is shown (Figs. 1a, b, c) in measurements of Garriott, et al (Ref. 8). The data is derived from observations on the Faraday rotation of signals of Syncom III at the University of Hawaii during the fall of 1964. These show an order of magnitude variation in the diurnal excursion of N_t with a steep morning rise and evening decay. The day-to-day variations in the amplitude of the mid-day maximum are about 25% and more.

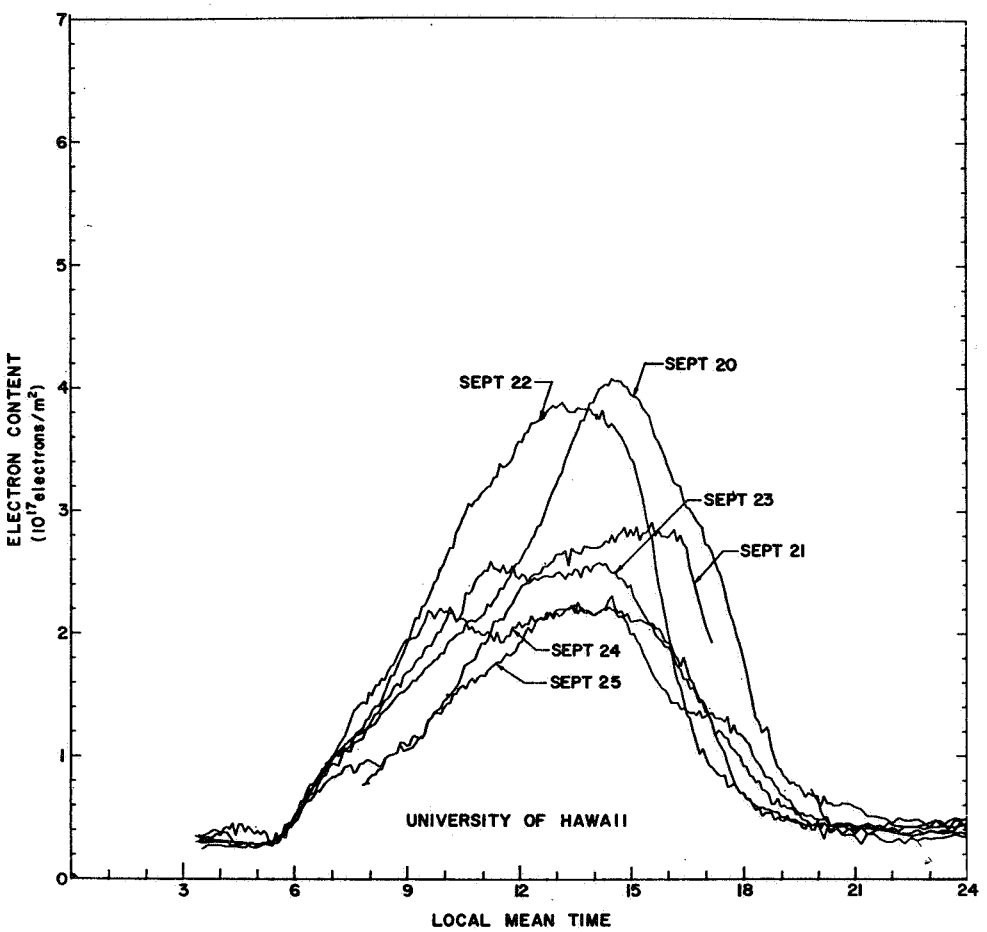

Figure 1(a)—Diurnal variation of electron content at the University of Hawaii for September 20-25, 1964, inclusive. [From Garriott, et al., Ref. 8].

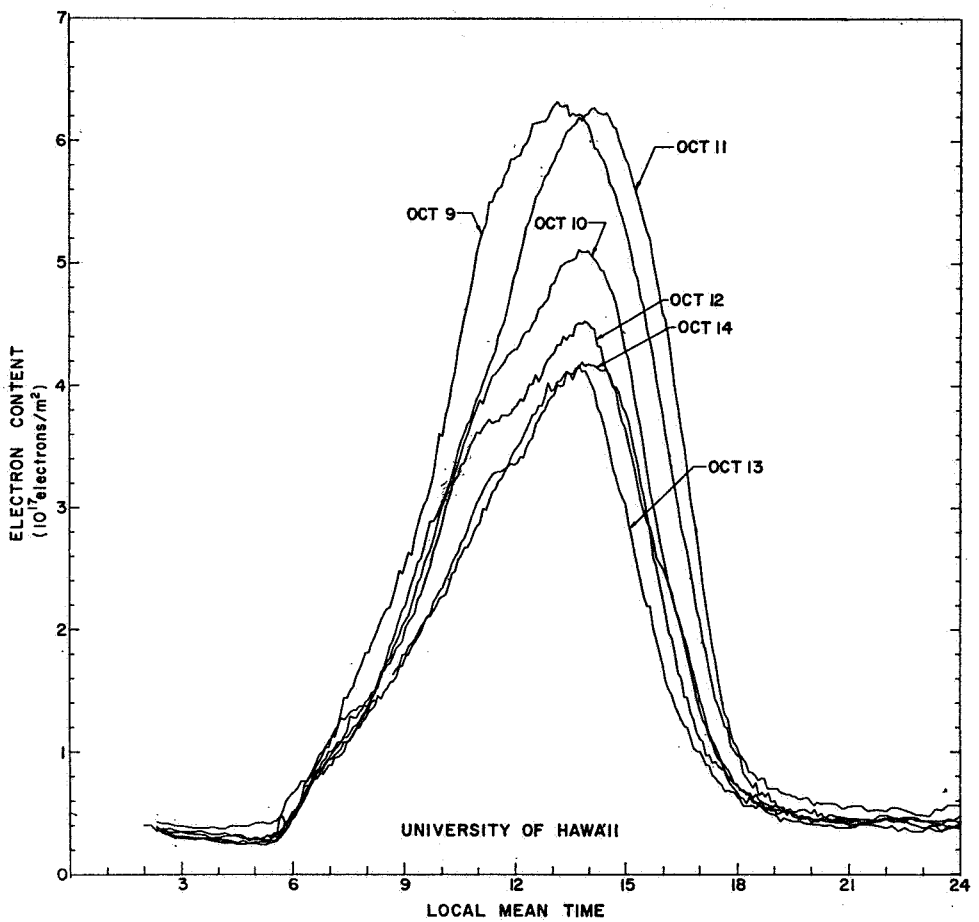

Figure 1(b)—Diurnal variation of electron content at the University of Hawaii for October 9-14, 1964, inclusive. [From Garriott, et al., Ref. 8].

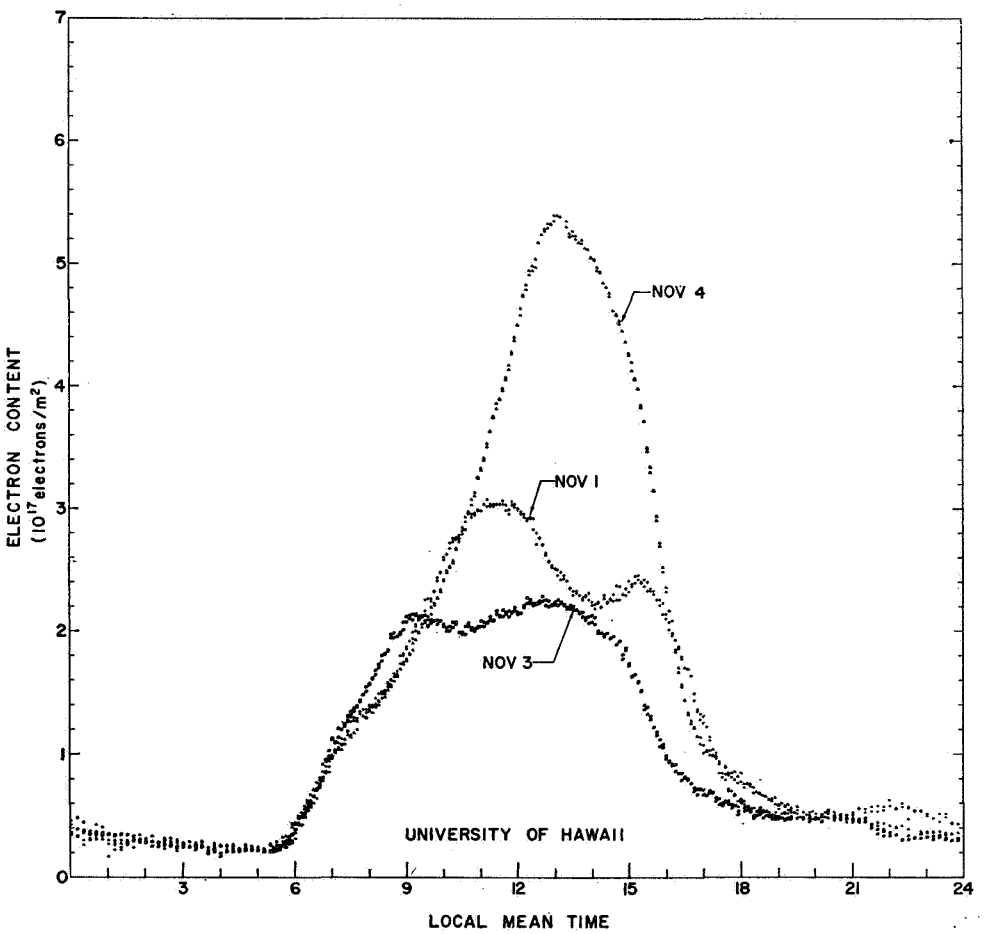

Figure 1(c)—Diurnal variation of electron content at the University of Hawaii for November 1, 3, and 4, 1964. These days were selected to illustrate the large day to day and even hour to hour variability sometimes observed. Yet, the nighttime and sunrise portions remain nearly identical. Individual data points are also shown. [From Garriott, et al., Ref. 8].

Geographic location has a significant influence on diurnal patterns. Observations of Schmerling (Ref. 9) during the summer of 1957 made on bottomside ionospheric profiles show very marked dissimilarity for three different sounding locations (Huancayo, Talara, and Panama) in the equatorial zone near a common meridian; the diurnal maximum at these stations occurred, respectively, at morning, midnight, and evening.

In addition to the diurnal cycle and geographical location, the ionosphere varies widely through the course of the eleven year solar sunspot cycle. The ionospheric medium is furthermore subject to irregular and abrupt changes under the influence of solar and geomagnetic disturbances. These remarks are to point out the complex variability of the ionosphere. Indeed to describe the pattern and variability is to list in addition to regular features, hosts of anomalies and irregularities (Ref. 10 and 11).

The result of the varigated ionospheric behavior for tracking systems assumes differing forms corresponding to the tracking assignment or the application of the tracking data. For one, evaluating the effectiveness of ionospheric corrections is very difficult. The designation of a mission tracking error model can also be quite perplexing. Where there is a critical tracking interval, as say, in support of a spacecraft maneuver, the mission planner is apt to be conservative and take a pessimistic perturbation model for the analysis. We emphasize that this tendency – of exaggerated error estimate – amounts essentially to a downgrading of the tracking system expectation where the demand on performance is especially needed. The uncertainties associated with the ionosphere also exert an influence on

Minitrack, where there is the aforementioned practice of selective use of tracking data restricted to within 20° of the zenith. Though refraction errors are thereby minimized it is at the expense of a substantial rejection of tracking data. That such restrictions can be excessive appears in the GEOS-I tests on Minitrack. This will be described below.

The refraction correction applied to Minitrack data are based on a horizontally stratified ionospheric model. With emphasis on small zenith angles, the refraction is generally a small perturbation. The character of the ionospheric data is then of less significance. However, one may question the validity of the refraction model itself. It is evident from the dependence of ionospheric structure on solar zenith angle that the medium is not horizontally stratified. This implies a finite refraction for tracking at the zenith. The effect has not as yet been studied for Minitrack.

Now let us look at how these considerations relate to matters on the analysis of Minitrack data. Minitrack is routinely relied upon for tracking and orbit determination as an integral part of satellite experiments. Physical problems like these pertaining to the harmonics of the geopotential field and satellite drag also enter in the satellite equations of motion. How the ionosphere can interfere in orbital computations is shown in a study of Gooding (Ref. 12) on Ariel 2 (1964). Using Minitrack data, residuals between observation and calculated orbital position were 1' to 2' arc ($\sim$ 0.3 mr to 0.6 mr). It was difficult to explain the magnitude of the residuals when the instrumental precision of Minitrack (Ref. 13) is 10^{-4} in direction cosine or 20" arc (0.1 mr) at the zenith.

The discrepancies were attributed to errors, real or apparent, having several possible sources, mainly ionospheric refraction, atmospheric drag, and uncertainty in the magnitude of the tesseral harmonics entering in orbital calculation. In the effort to evaluate these factors, Gooding, left the question of ionospheric refraction substantially unresolved. Significantly this was a period near solar minimum when ionospheric effects are smallest. This shows the uncertainty prevailing on the part of an investigator in approaching the ionospheric problem.

As a part of the GEOS-I program, a study was made to validate the accuracy of Minitrack measurements (Ref. 2). The test data were tracking observations on the GEOS satellite over a five day period, Dec. 31, 1965 to Jan. 5, 1966. This was in an early ascending phase of the solar cycle (Wolf sunspot number ~ 40) when the ionospheric electron content is still relatively low. The satellite was in a near drag-free orbit (perigee ~ 1200 km and apogee, ~ 2500 km). A standard orbit based on highly precise optical observations was available for intercomparison with Minitrack test data. The treatment of this data differed in several respects from the usual routine of Minitrack. Although accurate orbital calculations are limited to data observed within 20° of the zenith, the data acquisition in the test was extended to zenith angles of 75°. In addition, ionospheric refraction corrections were not applied to the data. The result in general showed a gratifying agreement in the residuals between Minitrack data and the optically determined standard orbit to within $\sim 0.2 \times 10^{-3}$ which compares with instrumental precision of 0.1×10^{-3} in the direction cosine.

This is a substantial corroboration of Minitrack precision. To achieve further refinement in Minitrack orbits, the ionospheric refraction must be corrected. But to validate Minitrack data we have yet to resolve the significance of horizontal gradients for refraction. The emphasis on observations near the zenith places importance on a general analysis of refraction effects at small zenith angles.

A principal objective of this report is therefore to investigate the contribution of ionospheric horizontal gradients to refraction and also their significance for GRARR ranging and range-rate perturbations. As part of this study we review ionospheric observational data relevant to these gradients. We describe the level of the various ionospheric perturbations on STADAN tracking accuracy.

The theory of refraction and of Doppler frequency shift in a heterogeneous ionospheric medium given herein follows substantially that of Al'pert (Ref. 14) and Mityokova and Mityakova (Ref. 15). Tropospheric effects in STADAN tracking have been studied by Freeman (Ref. 16) and are not considered here.

The principal difficulty for making meaningful corrections to ionospheric tracking errors stems from the variability of the medium. In order to cope with this problem there is no choice but to monitor suitable parameters of the ionosphere. A general result emerging from the analysis on tracking perturbations is the central role of N_t and its horizontal gradients. This then guides us to what should be monitored. We suggest in the concluding section with brief remarks how a synchronous orbiting satellite might serve in support of this monitor.

We treat in the next part the ionospheric perturbations on range, refraction, and range-rate (Doppler frequency shift) in that order. In the succeeding part we examine ionospheric data from the literature on horizontal gradients or N_t.

II. IONOSPHERIC TRACKING PERTURBATIONS AT VHF

Range

The VHF system of GRARR performs ranging by measurement of the propagation delay of sidetones impressed on the carrier signal. In the two two-way propagation, the uplink carrier frequency f_1 is approximately 148 MHz and the downlink frequency f_2 approximately 136 MHz. The ionospheric range perturbation ΔR_c is given by the integral

$$\Delta R_c = \frac{c}{2} \int_0^{s_c} \left(\frac{1}{v_{g1}} + \frac{1}{v_{g2}} \right) ds - \int_0^{s_c} ds \tag{1}$$

taken along the ray path S_I where c is the speed of light, ds the element of path length, s_c the path length between station position o and satellite position c, and v_{g1} and v_{g2} the group velocities of the carrier signals.

Group velocity is determined by the relation (Ref. 22)

$$\frac{c}{v_g} = \mu + f \frac{\partial \mu}{\partial f} \tag{2}$$

where μ is the refractive index of the ionosphere. Neglecting the earth's magnetic field, μ is

$$\mu = \sqrt{1 - \frac{80.6\, N_e}{f^2}} \tag{3a}$$

N_e is electron density (e/m^3) and f is in mHz. To a sufficient approximation at VHF

$$\mu = 1 - \frac{40.3\, N_e}{f^2} \equiv 1 - \eta N_e \tag{3b}$$

The numerical values of the parameter η are

$$\begin{array}{lll} \text{uplink} & \eta_1 = 18.4 \times 10^{-16}, & f_1 = 148 \text{ mHz} \\ \text{downlink} & \eta_2 = 21.8 \times 10^{-16}, & f_2 = 136 \text{ mHz} \end{array} \tag{4}$$

From the above equations, we have for the range perturbation

$$\Delta R_c = \eta \int_0^{s_c} N_e \, ds \tag{5a}$$

where (in this section) $\eta = 1/2\ (\eta_1 + \eta_2)$. The integral of Eq. (5) is an integrated electron content along the ray path, denoted by n_t (e/m^2). Thus

$$\Delta R_c = \eta\, n_t \tag{5b}$$

The bending of the ray path, being second order in the refractivity, can be neglected and n_t evaluated along the rectified path.

$\underline{z_c \geq 700 \text{ km}}$. Consider the case of satellite altitudes z_c above the ionosphere.

We write Eq. (5) in the form

$$\Delta R_c = \eta \int_{r_0}^{r_c} N_e \frac{dr}{\cos \phi} \tag{5}$$

where

$dr = ds \cos \phi$

r = radial distance from the earth center

ϕ = angle between ray path S and the radial line

r_0 = earth radius

$r_c = r_0 + z_c$

The predominant contribution to the integral of Eq. (5) comes in an altitude interval about N_{max} (maximum of N_e). Since the geometric factor $(\cos \theta)^{-1}$ is a slowly varying function we can make the approximation of removing the factor from under the integral sign and assigning an appropriate mean value corresponding to a point m:

$$\Delta R_c = \frac{\eta}{\cos \phi_m} \int_{r_0}^{r_t} N_e \, dr = \frac{\eta N_t (\theta_m)}{\cos \phi_m} , \tag{7}$$

The point m is at the median for the electron content along the path from o to c; θ_m is the polar angle at the earth center of the point m relative to o. We designate m as the ionospheric point and its projection on the earth's surface as the sub-ionospheric point corresponding to the ray path. Thus, ΔR_c can be expressed in terms of $N_t (\theta_m)$, the total integrated electron content at the sub-ionospheric point.

In the northern mid-latitude region the altitude z_m is variable, but typically about 350 km during daylight hours. Due to uncertainty in determining this altitude there is an error introduced in the evaluation of Eq. (7). This we now shall consider. From the geometry of Fig. 2

$$r \sin \phi = r_0 \sin \phi_0 = r_m \sin \phi_m \tag{8}$$

and

$$\tan \phi = \frac{r d\theta}{dr} = \frac{dx}{dr} \tag{9}$$

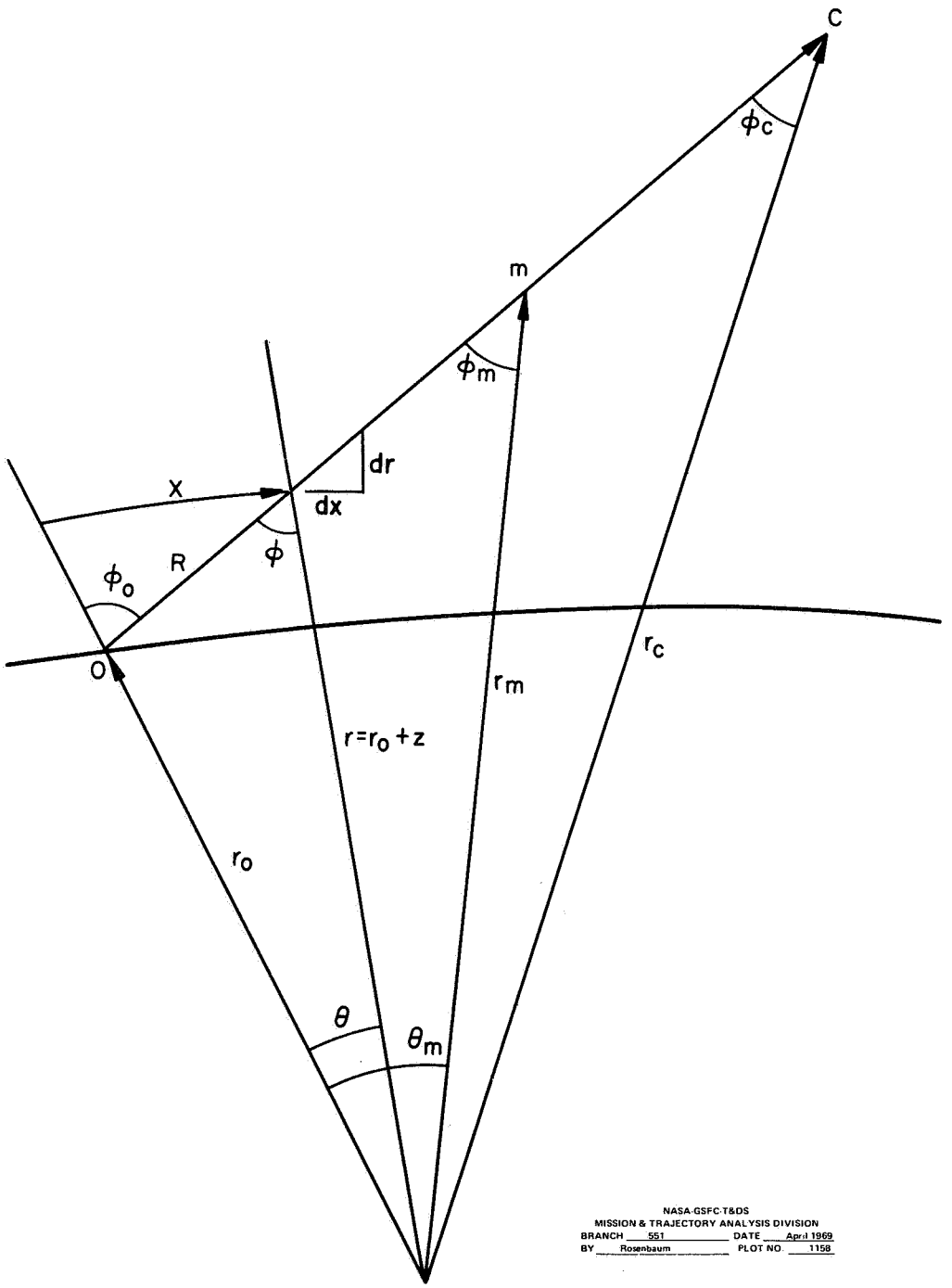

Figure 2—Plane of incidence.

where x is the horizontal curvilinear distance. Using Eqs. (7) and (8) we have as the error in ΔR_c from an uncertainty Δr_m $(=\Delta z_m)$

$$- \eta N_t \frac{\tan^2 \phi_m}{\cos \phi_m} \frac{\Delta r_m}{r_m} + \eta \frac{\partial N_t}{\partial x} \frac{\tan \phi_m}{\cos \phi_m} \Delta r_m \tag{10}$$

The relative error is

$$- \tan^2 \phi_m \frac{\Delta r_m}{r_m} + \frac{1}{N_t} \frac{\partial N_t}{\partial x} \tan \phi_m \Delta r_m \tag{10a}$$

It is reasonable to take $\Delta r_m = 50$ km since this representative of the uncertainty in r_m. At zero elevation angle, (10a) is a maximum. Then with $z_m = 350$ km, Eq. (7) gives $\tan \phi_m \doteq 3$. The first term in (10a) is 7%; and the second is 1% for an above average logarithmic gradient $1/N_t \cdot \partial N_t/\partial x = 5 \times 10^{-4}$ $(\text{km})^{-1}$.

Bounds of N_t. To see how the ionosphere controls the magnitude of ΔR_c we need to know the bounds on the variation of N_t. There are numerous factors influencing N_t, the principal ones being the eleven year sunspot cycle and the diurnal cycle. There has been observed, in the northern mid-latitude region, a very useful empirical relation between the mid-day peak, $(N_t)_{max}$, of N_t and the mean sunspot number $\overline{R}$. Fig. 3 (Ref. 17) shows the composite of data from a number of investigators. There is an approximate linear relation between $(N_t)_{max}$ and $\overline{R}$ for the seasons of the year for $\overline{R} > 40$; and for $\overline{R} < 40$, $(N_t)_{max}$ levels off at minimum of about 1×10^{17} e/m^2.

The maximum of $(N_t)_{max}$ is 10^{18} e/m^2. The observed and predicted R vs time is given in Ionospheric Predictions. This dependence is shown in Fig. 4 (Ref. 18).

The diurnal variation of N_t is about an order of magnitude. We can then give approximate extreme limits on the variation of N_t through the eleven year solar cycle. These are shown in Table I, with 10^{16} e/m^2 $\lesssim N_t \lesssim$ 10^{18} e/m^2.

Table I
Approximate Extreme Variations of N_t (e/m^2)
(Northern Mid-latitude Region)

	Diurnal Max.	Diurnal Min.
Sunspot Max.	10^{18}	10^{17}
Sunspot Min.	10^{17}	10^{16}

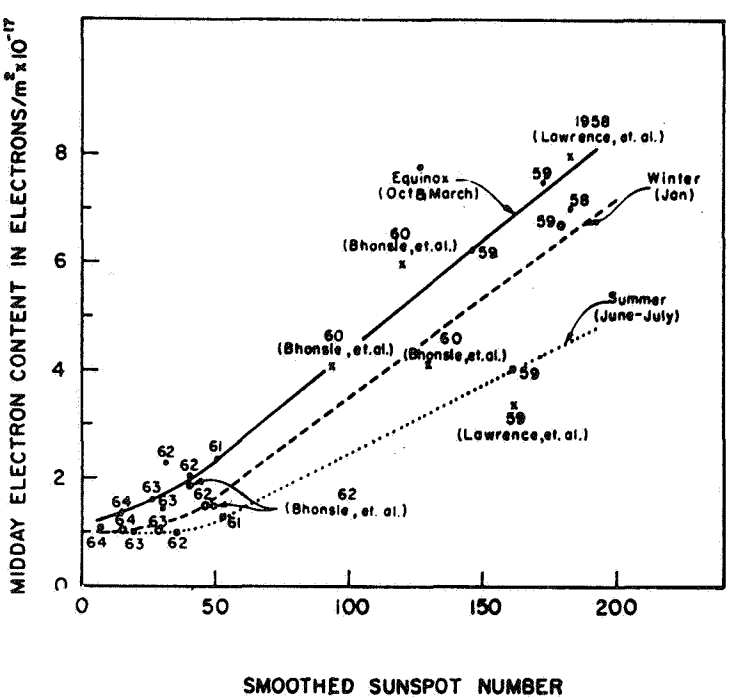

Figure 3—Sunspot dependence of midday electron content. [From Yeh, et al, Ref. 17].

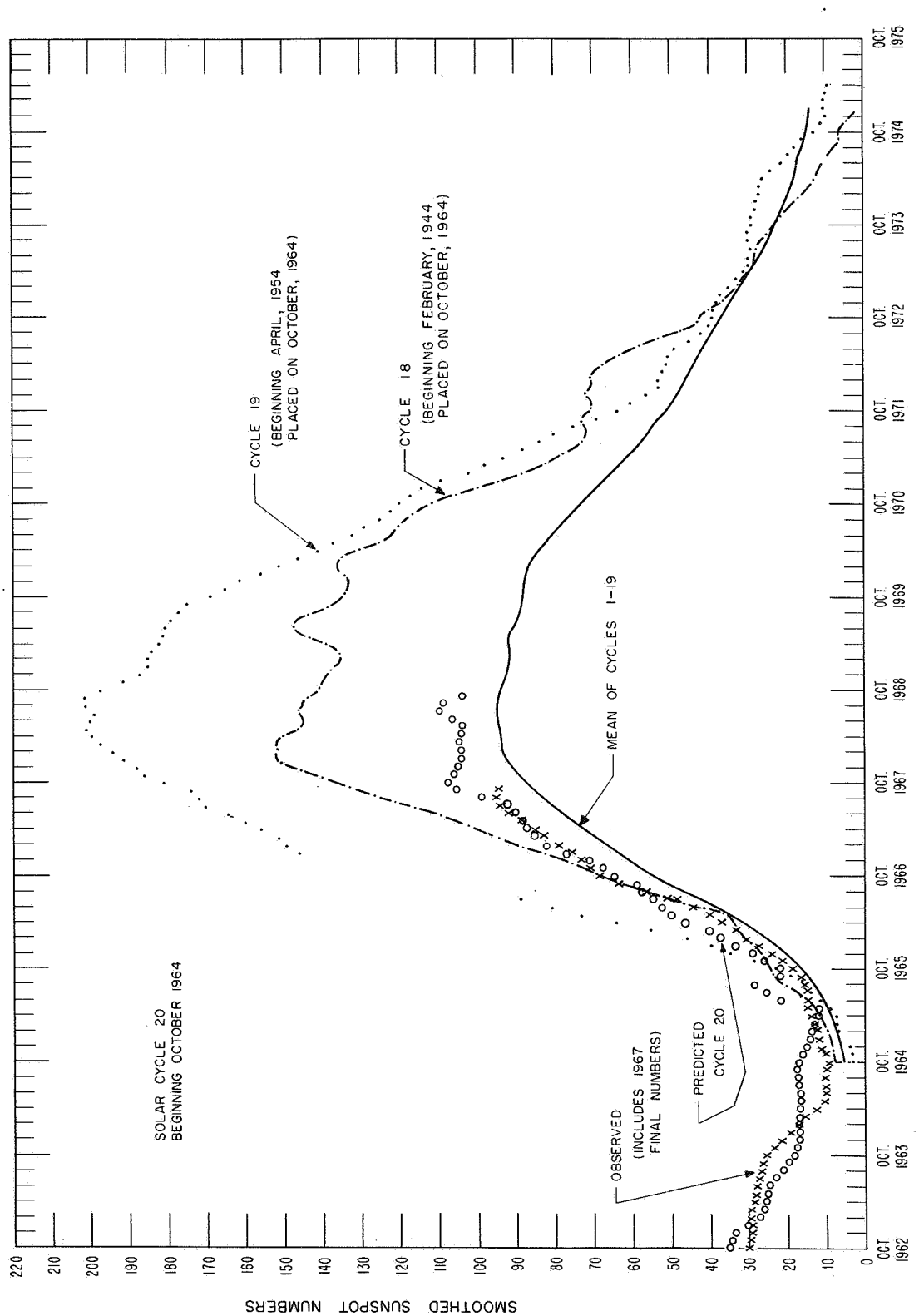

Figure 4—Predicted and observed sunspot numbers. [From Ref. 18].

The dependence on zenith angle is obtained by combining Eqs. (7) and (8). Thus

$$\Delta R_c = \frac{\eta N_t(\theta_m)}{\sqrt{1 - \frac{r_0^2 \sin^2 \phi_0}{r_m^2}}} \tag{11}$$

or

$$\Delta R_c = \frac{\eta N_t(\theta_m)}{\sqrt{1 - 0.88 \sin^2 \phi_0}} \tag{12}$$

for the mediam altitude $z_m = 350$ km. At the zenith the range ΔR_c is, according to Table I, between the approximate bounds 20 meters and 2000 meters. At the horizon ΔR_c is 2.7 times that at the zenith.

This perturbation on ΔR_c is to be compared to the GRARR instrumental precision which, at the highest sidetone (for VHF), 20 kHz, is nominally 14 meters (Ref. 1).

Refraction

In this section the theory of refraction in a heterogeneous ionospheric medium (Ref. 14) will be applied to Minitrack.

It is convenient to describe the refraction with respect to the plane of incidence, I, defined by the observer, o, satellite position, c, and the earth center. The geometry is shown in Fig. 5. In the presence of horizontal

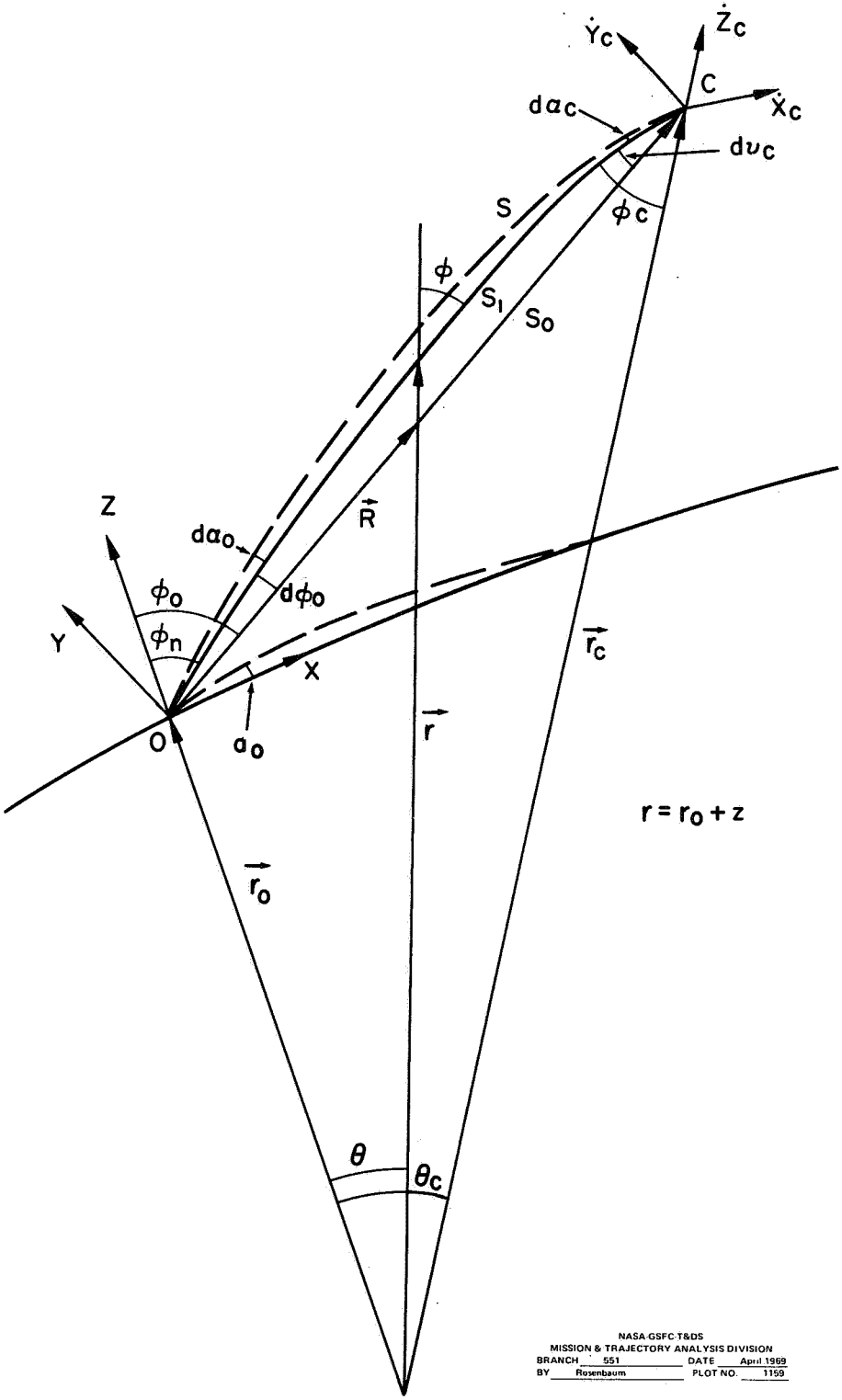

Figure 5—Three dimensional refraction geometry.

ionospheric gradients, the ray path S from o to c deviates from the plane I. The projection of S onto I is denoted by S_I, while S_0 is the line-of-sight. The angles θ and ϕ in the plane I are as previously defined in connection with Fig. 2. The horizontal curvilinar coordinate y measures the small deviations of S normal to I, such that x, y, and z form a right-handed system.

At the observer, the refraction of the zenith angle $d\phi_0$ measured in I is given by

$$d\phi_0 = \phi_n - \phi_0 \tag{13}$$

where ϕ_n and ϕ_0 are zenith angles respectively of S_I and S_0. The refraction angle of S at o normal to I, that is the angle between S and S_I, is denoted by $d\alpha_0$. The relation to the azimuthal refraction angle a_0 is

$$da_0 = \frac{d\alpha_0}{\sin \phi_0} \tag{14}$$

Minitrack determines the angular position of a satellite from observation on the arrival direction of the satellite beacon (downlink, $f_1 = 136$ MHz) signal. A crossed pair of interferometers having a east-west (equatorial) and north-south (polar) orientations measure direction cosines, cos γ and cos β, respectively. The connection between Minitrack observations and the refraction theory is through the equations (Fig. 6)

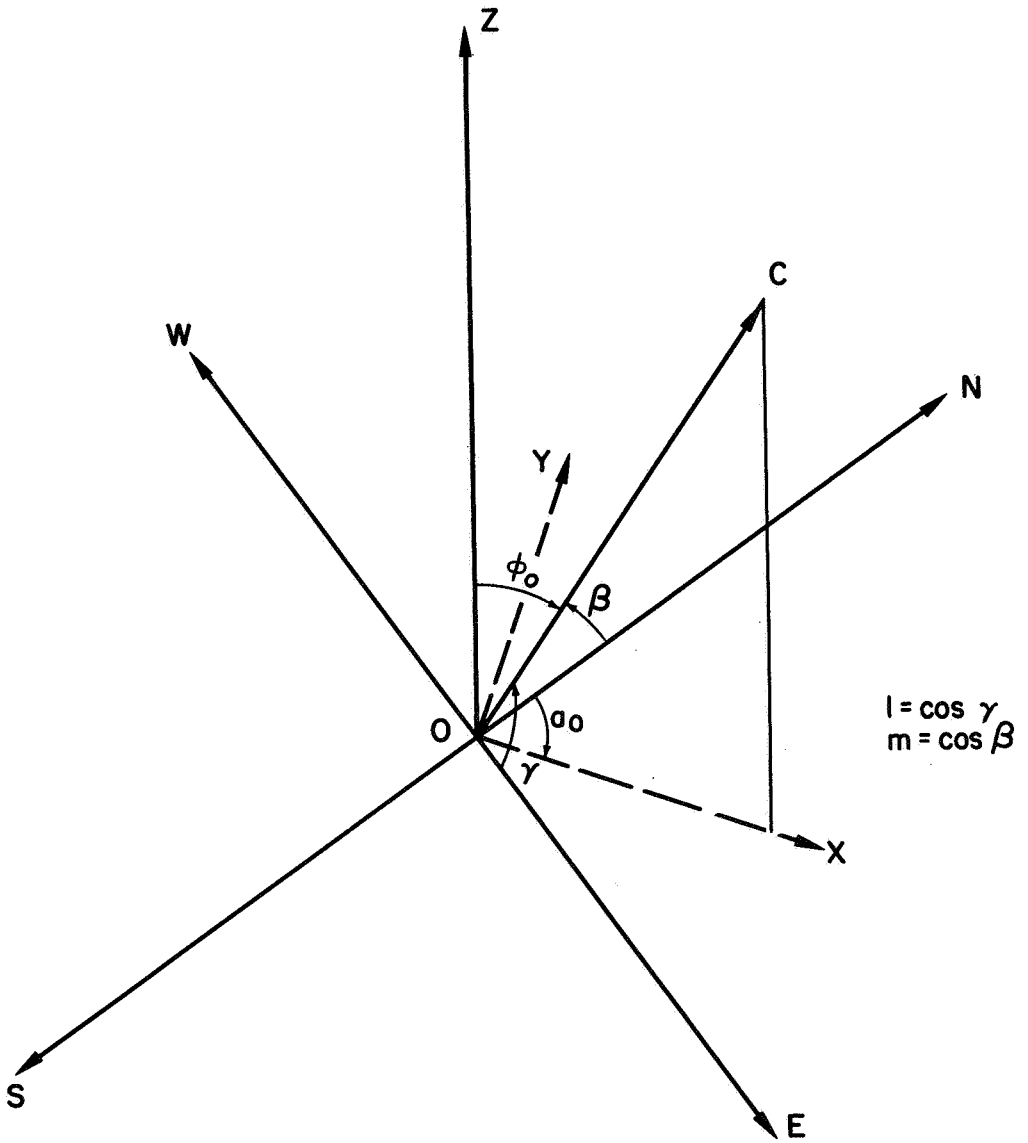

Figure 6—Minitrack angles.

$$\cos\beta = \sin\phi_0 \cos a_0$$
$$\cos\gamma = \sin\phi_0 \sin a_0 \qquad (15)$$

where a_0 is the azimuthal angle.

The calculation of the refraction is based on the Fermat Principal that the radio phase path Φ between emitter and receiver is minimum, that is,

$$\delta\Phi = \frac{2\pi f_0}{c} \delta \int_0^t \mu \, ds = 0 \qquad (16)$$

where the index of refraction $\mu = 1 - \eta N_e$ (x, y, z). (For Minitrack, $\eta = \eta_2$ of Eq. (4).) The calculation is given in Appendix I where it is shown that

$$d\phi_0 = -\frac{\eta r_0 r_c \sin\phi_0 \cos\phi_c}{R_c} \int_{r_0}^{r_c} \frac{N_e \, dr}{r^2 \cos^3\phi} + \eta \int_0^{R_c} \frac{\partial N_e}{\partial x} \frac{(R_c - R)}{R_c} \frac{dR}{\cos\phi} \qquad (A22)$$

$$d\alpha_0 = \eta \int_0^{R_c} \frac{\partial N_e}{\partial y} \frac{(R_c - R)}{R_c} \, dR \qquad (A26)$$

The integrals are taken along the line-of-sight path, S_0, and R is distance from o. These expressions have been given by Mityakova and Mityakova (Ref. 15). The restriction is that

$$\cos^2\phi >> \eta N_e \qquad (17a)$$

$$\eta \left| \int_0^{R_c} \frac{\partial N_e}{\partial x} ds \right| \ll \cos^2 \phi_0 \tag{17b}$$

and

$$\eta \left| \int_0^{R_c} \frac{\partial N_e}{\partial y} ds \right| \ll 1. \tag{17c}$$

The first term on the right side of Eq. (A22) is that associated with a spherically stratified medium (Ref. 19, 4). For tracking above the ionosphere, $z_c \gtrsim 700$ km, this term, denoted as $d\phi_0^{(1)}$, can be approximated as

$$d\phi_0^{(1)} = - \frac{\eta \, r_0 \, r_c \sin \phi_0 \cos \phi_c \, N_t \, (\theta_m)}{R_c \, r_m^2 \cos^3 \phi_m} \tag{18}$$

where parameters with subscript m are evaluated at the ionospheric point along the ray path. For satellite within the ionosphere N_t is replaced by the sub-satellite electron content, with a small correction to the position of point m.

The relative error introduced in the approximation of Eq. (18) for an uncertainty, Δr_m, is

$$(2 + 3 \tan^2 \phi_m) \frac{\Delta r_m}{r_m} + \tan \phi_m \, \Delta r_m \frac{\partial N_t}{\partial x} \frac{1}{N_t}. \tag{19}$$

Taking $\Delta r_m = 50$ km, $\tan \phi_m = 1$ and $1/N_t \, \partial N_t / \partial x = 5 \times 10^{-4}$ (km^{-1}), this gives errors of 4% and 2.5% for the first and second terms, respectively.

For small zenith angle, $\phi_0 < 20°$ the expression for $d\phi_0^{(1)}$ may be further simplified to

$$d\phi_0^{(1)} \doteq - \frac{\eta N_t \tan \phi_0 \, (r_0 + z_c)}{r_0 \, z_c} \tag{20}$$

Thus $d\phi_0$ vanishes at the zenith as $\tan \phi_0$.

The maximum of $d\phi_0^{(1)}$ is at some altitude generally below 700 km depending on the vertical profile of N_e, while in the asymptotic limit for large z_c, $d\phi_0^{(1)} = \eta N_t \tan \phi_0 / r_0$. This limit is about an order of magnitude less than the maximum value at ionospheric altitudes.

There is given in Table 2 the perturbation on the cosine of the elevation angle, $d (\sin \phi_0)^{(1)} \equiv \cos \phi_0 \, d\phi_0^{(1)}$ (based on Eq. (18)) as a function of satellite altitude for zenith angles, $\phi_0 = 20°$ and 45° and $N_t = 10^{18}$ e/m^2. The tabulation can be used in conjunction with Table 1 to estimate variations of the refraction effect corresponding to extremes of the 11 year solar cycle and diurnal cycle. For an earth orbiting vehicle of, say, 1000 km altitude, the following are some general conditions under which the perturbation is apt to

Table 2

$-d\ (\sin \phi_0^{(1)}) \times 10^3$ for $N_t = 10^{18}$ e/m^2

z_c (km/ϕ_0	20°	45°
350	~0.4	~2
750	~0.34	~2.0
1000	0.28	1.6
2000	0.17	1.05
3000	0.12	0.83
r_0	0.08	0.61
$2r_0$	0.06	0.50
∞	0.04	0.39

exceed 10^{-4}. At $\varphi_0 = 45°$ for daytime and nighttime ionosphere of the sunspot maximum and also for the daytime of the solar minimum; while at $\varphi_0 = 20°$ for the daytime ionosphere of the solar maximum and also for the midday ionosphere of intermediate sunspot number. This then is descriptive of refractive errors in Minitrack due to the first term of Eq. (A22).

The second term in Eq. (A22), which we denote as $d\phi_0^{(2)}$, and $d\alpha_0$ of Eq. (A26) give, respectively, the refractive contributions of the horizontal gradients in and normal to the plane of incidence. As these are similar in form it will suffice to discuss only one. We choose

$$d\phi_0^{(2)} \equiv \eta \int_{r_0}^{r_c} \frac{\partial N_e}{\partial x} \frac{(R_c - R)}{R_c} \frac{dr}{\cos^2 \phi} \qquad (21)$$

We assign to the geometric factor in Eq. (21) a mean value corresponding, approximately, to m', the median point of $\partial N_e/\partial x$ along the integration path. Thus

$$d\phi_0^{(2)} \doteq \frac{\eta (R_c - R_{m'})}{R_c \cos^2 \phi_{m'}} \int_{r_0}^{r_c} \frac{\partial N_e}{\partial x} dr \tag{22}$$

or for z_c above the ionosphere

$$d\phi_0^{(2)} \doteq \frac{\eta (R_c - R_{m'})}{R_e \cos^2 \phi_{m'}} \frac{\partial N_t}{\partial x} \tag{23}$$

where $R_{m'}$ is the distance from o along S of the point m' corresponding to the altitude $z_{m'}$. Note that cos $\phi_{m'}$ is determined by Eq. (7). Thus Eq. (23) relates $d\phi_0^{(2)}$ to the ionospheric parameter, $\partial N_t/\partial x$ and $z_{m'}$. Consideration of ionospheric behavior shows that the gradient of N_t varies extensively, while $z_{m'}$ has a more restricted variation. The latter parameter would appear to be approximated by z_m, since at least for simple ionospheric theory like the Chapman model, $\partial N_e / \partial x \sim N_e$. Accordingly, by Eq. (23) the principal ionospheric parameter needed for calculating $d\phi_0^{(2)}$ (and likewise, $d\alpha_0$) is the gradient of N_t when satellite is above the ionospheric layer.

At lower altitudes the treatment of Eq. (22) is modified. As a rule, $d\phi_0^{(2)}$ is not large; the maximum for the strongest observed ionospheric gradients is within an order of magnitude of Minitrack precision. Furthermore, for z_c decreasing to ionospheric altitudes, $d\phi_0^{(2)}$ decreases substantially. In this altitude regime any expression of $d\phi_0^{(2)}$ corresponding to form of Eq. (23) has as its gradient factor $\partial n_t(z_c)/\partial x$ and the median point corresponding to $R_{m'}$ shifted.

Accuracy requirement on these parameters can be relaxed considerably due to the diminished magnitude of $d\phi_0^{(2)}$. Accordingly if $\partial N_t/\partial x$ and R_m, of Eq. (23) are known there should not be serious difficulty in treating the lower altitude case.

The main assumption of the ionosphere leading to these remarks is that the horizontal gradients of N_e are near maximum in altitudes near z_m. To get a better look at this, one needs observational data on vertical and horizontal profiles of N_e. However, such data is scarce, at least in journal publications. We do find topside and bottomside data, but at differing periods of observation. The sample we shall discuss gives latitudinal gradients of $N_e(z)$ for daylight hours. These are the conditions under which the horizontal gradients are generally largest. Observations of the bottomside profiles by Wright (Ref. 20) were made during IGY. The observations were near the 75°W meridian in the latitude interval 15°N to 50°N. The data show mean ionospheric behavior for the month of Aug. 1959 at 1700 LMT. The latitudinal gradient is negligibly small except for the altitude interval of 50 km bordering h_{max}.

Extensive synoptic observations of the topside have been made by Alouette I. Data on latitudinal variations of N_e profiles near the west 75° meridian are reported by Chan (Ref. 22). Two sets of observations under differing geomagnetic conditions are shown in Figs. 7a and 7b; respectively, one for June 7, 1962 at local time between 1100 and 1430, and the other for Oct. 31, 1963 at local time between 1600 and 2200. These data show the maximum level of N_e at the geomagnetic

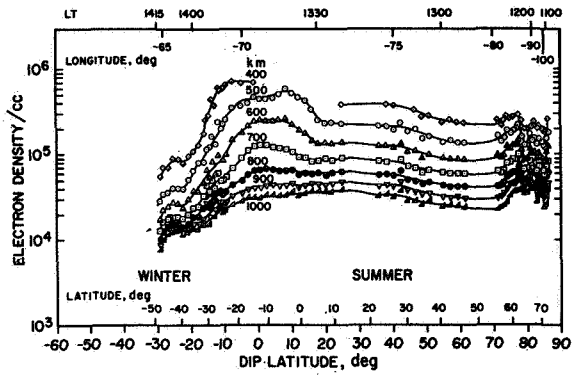

Figure 7(a)—Latitudinal variation of electron density on June 7, 1963 (Pass 3432; 1757 to 1836 UT; Kp = 4⁻ to 3°). [From Chan, Ref. 21].

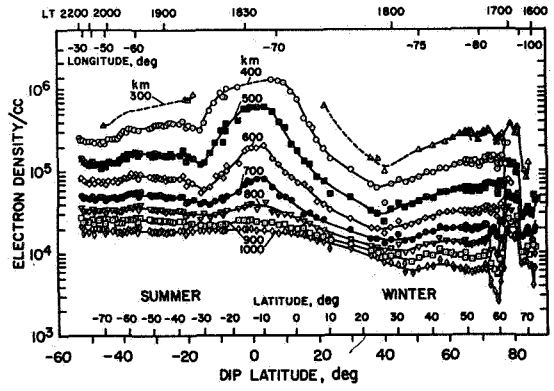

Figure 7(b)—Latitudinal variation of electron density on October 31, 1963 (Pass 5427; 2239 to 2326 UT; Kp = 1⁻). [From Chan, Ref. 21].

equator with gradients extending into the midlatitude regions. The horizontal gradients of N_e are seen to be a maximum near h_{max}. The median altitude of the gradient, $z_{m'}$, is about 100 km above h_{max}. If we consider a model with the combined features of data of Wright and Chen then we would have $z_{m'} \sim h_{max}$ + 100 km. The example is at least consistent with the notion $z_{m'} = z_m$.

Criteria on gradient of N_t. The evaluation of $d\phi_0^{(2)}$, according to Eq. (23) depends on $\partial N_t/\partial x$. The magnitude variations of this ionospheric parameter will be the subject of the next section. Here we will establish criteria indicating whether the gradients are a relevant factor for perturbation on Minitrack observations. For making an apt comparison with Minitrack precision, we consider $d(\sin \phi_0)^{(2)}$ ($\equiv \cos \phi_0 \, d\phi_0^{(2)}$); that is,

$$d(\sin \phi_0)^{(2)} = \frac{\eta \cos \phi_0}{\cos^2 \phi_{m'}} \frac{(R_c - R_{m'})}{R_c} \frac{\partial N_t}{\partial x} \tag{24}$$

This term, in contradistinction to $d\phi_0^{(1)}$, does not vanish at the zenith and furthermore increases asymptotically with range.

For a rough numerical estimate of Eq. (24) it is acceptable to write

$$d(\sin \phi_0)^{(2)} \cong 2.2 \times 10^{-5} \frac{\cos \phi_0}{\cos^2 \phi_{m'}} \frac{(z_c - z_{m'})}{z_c} \frac{\partial N_t}{\partial x} \tag{25}$$

where we have used $\eta = \eta_2$; the approximation, $R_{m'}/R_c \cong z_{m'}/z_c$; and $\partial N_t/\partial x$ is in gradient units (G.U. = 10^{13} e/m^2 km). Representative cases of interest are: $\varphi_0 = 0°$ and 45°; $z_c = 750$ km and $\geq 3r_0$. There is in Table 3, for these parameter values the minimum gradient of N_t for which $d\phi_0^{(2)}$ equals the Minitrack precision, 10^{-4}.

Table 3

$\partial N_t/\partial x$ (G.U.) for $d(\sin \varphi_0)^{(2)} = 10^{-4}$

ϕ_0/z_c	750 km	$\gtrsim 3r_0$
0°	9.0	4.4
45°	6.4	3.2

Range-Rate

In the GRARR system the satellite range-rate measurement is performed through a coherent two-way Doppler technique. But the system measures effectively the Doppler frequency shift of the uplink carrier signal frequency, f_1 (Ref. 41). Hence, we consider the one-way Doppler frequency shift, f_d, which in the non-relativistic approximation is for a time dependent ionospheric medium

$$-\frac{f_d}{f_1} = \frac{1}{c}\frac{d}{dt}\int_0^{s_c(t)} \mu(\vec{r},\ t)\, ds \tag{26}$$

Kelso (Ref. 22) has demonstrated that

$$-\frac{f_d}{f_1} = \frac{\mu(\vec{r}_c,\ t)\,\hat{\tau}_c\cdot\dot{\vec{r}}_c}{c} + \frac{1}{c}\int_0^{s_c}\frac{\partial\mu}{\partial t}\, ds \tag{27}$$

where $\hat{\tau}_c$ is the unit tangent vector to S at c. The first term on right side will not in general vanish at the point-of-closest approach in a three dimensionally heterogeneous ionosphere (as it would for a spherically symmetric medium) but instead vanishes at another point of the trajectory displaced from the former by a finite distance. The effect of the time dependent ionosphere is expressed by the second term in Eq. (27).

Utilizing the relation between the Doppler effect and satellite range-rate, the effects embodied in Eq. (27) can be represented as the sum of an unperturbed vacuum Doppler term, $\dot{R}_c/c$, and a term of ionospheric perturbation, $\Delta\dot{R}_c/c$; that is

$$-\frac{f_d}{f_1} = \frac{\dot{R}_c}{c} + \frac{\Delta\dot{R}_c}{c} \tag{28}$$

Correspondingly we rewrite Eq. (27)

$$-\frac{f_d}{f_1} = \frac{\hat{u}_0 \cdot \dot{\vec{r}}_c}{c} + \frac{(\mu_c - 1)\,\hat{\tau}_c \cdot \dot{\vec{r}}_c}{c} + \frac{(\hat{\tau}_c - \hat{u}_0)\cdot \dot{\vec{r}}_c}{c} + \frac{1}{c}\int_0^{s_c} \frac{\partial \mu}{\partial t}\, ds \tag{29}$$

where $\hat{u}_0$ is the line-of-sight unit vector between o and c. From the relation $\dot{R}_c = \hat{u}_0 \cdot \dot{\vec{r}}_c$ we have from Eqs. (28) and (29)

$$\Delta\dot{R}_c = (\mu_c - 1)\,\hat{\tau}_c \cdot \dot{\vec{r}}_c + (\hat{\tau}_c - \hat{u}_0)\cdot \dot{\vec{r}}_c + \int_0^{s_c} \frac{\partial \mu}{\partial t}\, ds \tag{30}$$

The effect due to local refractivity at c in the first term on the right is by Eq. (3b)

$$(\mu_c - 1)\,\hat{\tau}_c \cdot \dot{\vec{r}}_c = -\eta\, N_e(\vec{r}_c,\ t)\, \dot{R}_c \tag{31}$$

where we use the approximation $\hat{\tau}_c \approx \hat{u}_0$. ($\eta = \eta_1$ for formulas related to the Doppler measurements, hence to all formulas in this section where η appears.)

The second term of Eq. (30) is due to the effect of the finite refraction angle at c. We express this in component form (Fig. 8)

$$\dot{\vec{r}}_c \cdot (\hat{\tau}_c - \hat{u}_0) = v_\perp \chi_c = (R_c\, \dot{\phi}_0)\, d\phi_c + \dot{y}_c\, d\alpha_c \tag{32}$$

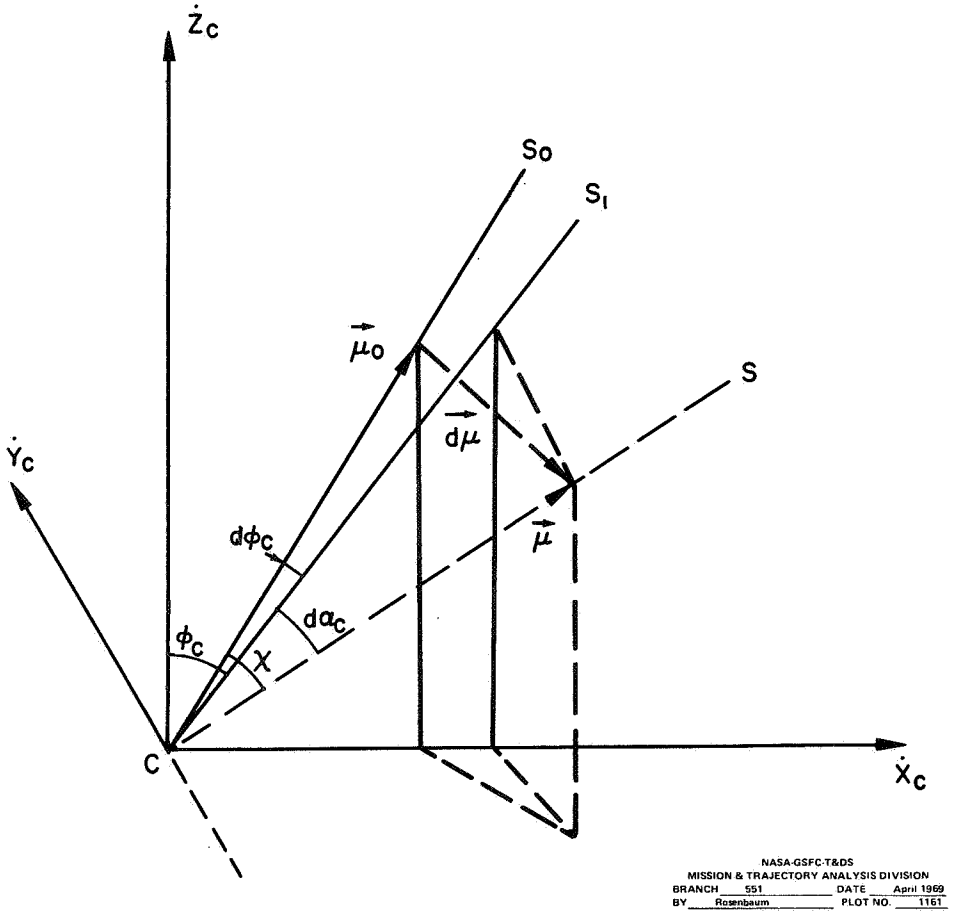

Figure 8—Refraction angles at C.

where

χ_c = angle between $\hat{\tau}_c$ and $\hat{u}_0$

$v_\perp$ = projection of $\dot{\vec{r}}_c$ on $\hat{\tau}_c - \hat{u}_0$

$d\phi_c$ = refraction angle at c between S_0 and S_I

$d\alpha_c$ = refraction angle between S and I-plane at c.

The Eqs. (30) and (32) show how the components of refraction of the ray path at c enter in the formula for ΔR_c.

The formula for the refraction angles are given in the Appendix B.

$$d\phi_c = -\frac{\eta\, r_0\, r_c \cos\phi_0 \sin\phi_c}{R_c} \int_{r_0}^{r_c} \frac{(N_e(\vec{r}) - N_e(\vec{r}_c))\, dr}{r^2 \cos^3\phi}$$

$$-\eta \int_0^{R_c} \frac{R}{R_c} \frac{\partial N_e}{\partial x} \frac{dR}{\cos\phi} \qquad \text{(A28)}$$

and

$$d\alpha_c = -\eta \int_0^{R_c} \frac{R}{R_c} \frac{\partial N_e}{\partial y}\, dR \qquad \text{(A29)}$$

Inserting the terms of Eqs. (31) and (32) into Eq. (30) and using Eqs. (A19), (A28), and (A29) along with the geometric relation (Fig. 9)

$$\dot{z}_c = \dot{R}_c \cos\phi_c - R_c \dot{\phi}_0 \sin\phi_c \qquad \text{(33)}$$

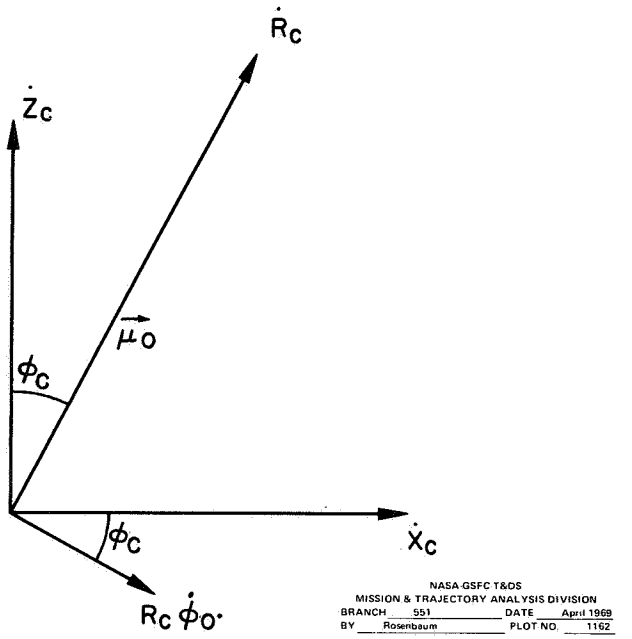

Figure 9—Velocity components in the l-plane.

we obtain

$$\Delta\dot{R}_c = -\eta\left\{\underbrace{\frac{\dot{z}_c\, N_e(\vec{r}_c)}{\cos\phi_c}}_{\text{I}} + \underbrace{\frac{(R_c\,\dot{\phi}_0)\, r_c\, r_0 \cos\phi_0 \sin\phi_c}{R_c}}_{\text{II}} \int_{r_0}^{r_c} \frac{N_e\, dr}{r^2 \cos^3\phi}\right.$$

$$\left. + (R_c\,\dot{\phi}_0) \underbrace{\int_0^{R_c} \frac{R}{R_c}\frac{\partial N_e}{\partial x}\frac{dR}{\cos\phi}}_{\text{III}} + \dot{y}_c \underbrace{\int_0^{R_c} \frac{R}{R_c}\frac{\partial N_e}{\partial y}\, dR}_{\text{IV}} + \underbrace{\int_{r_0}^{r_c} \frac{\partial N_e}{\partial t}\frac{dr}{\cos\phi}}_{\text{V}}\right\} \quad (34)$$

(The Roman numerals will serve to identify the various term of Eq. (34) for the discussion to follow in later paragraphs.)

It is worth noting that the expression of Eq. (34) can be also derived from Eq. (28) without introducing refraction angles (Ref. 15). Rewrite the integral of Eq. (28)

$$\frac{d}{dt}\int_0^{S_c}\mu\,ds=\frac{d}{dt}\int_0^{z_c}\frac{\mu(x,\,y,\,z)\,dz}{\cos\phi} \tag{35}$$

The point c and therefore the ray path are functions of time. Hence the parameters under the integral sign x, y and implicitly ϕ are time dependent. Thus, using Eq. (8),

$$\frac{d}{dt}\int_0^{S_c}\mu\,ds=\frac{d}{dt}\int_0^{z_c(t)}\frac{\mu\{x(t),\,y(t),\,z\}\,dz}{\sqrt{1-\dfrac{r_0^2\cos^2\phi_0(t)}{(r_0+z)^2}}} \tag{36}$$

where the time dependence is explicitly exhibited. By formal application of the time differential operation indicated in Eq. (36) and using geometric relations, the expression in the parethesis of Eq. (34) follows directly.

Discussion of $\Delta\dot{R}_c$. Table 4 lists approximate formulas for estimating the terms (II-IV) of Eq. (34) at satellite altitudes, 700 km $\lesssim z_c \lesssim r_0$, and large elevation angle. The formula for term V requires $z_c \gtrsim 700$ km. There is also given an

approximate magnitude level the terms can attain under the condition of maximum ionospheric electron content and maximum horizontal gradient.* The term values are to be compared with the instrumental range-rate precision of 6 cm/sec at a sampling interval of one sec (Ref. 1).

Term I is the local medium effect, which is maximum when at the altitude, $z_c = h_{max}$. Term II is a maximum at the top of the ionosphere. This vanishes, however, at the zenith and at the point-of-closest approach ($\dot{\varphi}_0 = 0$). Term III which is dependent on gradients in the I-plane is commonly an order of magnitude less than term II. It vanishes at $\dot{\varphi}_0 = 0$. Term IV is comparable in magnitude with III, but need not vanish at the zenith or at the point of closest approach.

At lunar range, the satellite angular velocity is so small that terms I to IV are negligible, in which case V can be the dominant term. The latter term is then a measure of the time rate of change of electron content along the essentially fixed line-of-sight. This may be due to short term fluctuation of the ionosphere or due to the diurnal cycle. For the steep diurnal changes of N_t and low elevation angles, the term can amount to about 50 cm/sec.

The approximate upper magnitude levels of the various terms of Table 4 is one to two orders of magnitude greater than instrumental error.

*The magnitude of horizontal gradients is treated in the next section.

Table 4
Terms of $\Delta\dot{R}_c$, Eq. (34)

Term	Term Approximation (m/sec)	Upper Magnitude Level (m/sec)
I	$\frac{2 N_{e,c} \dot{z}_c}{\cos \varphi_c}$	20
II	$\frac{10^{-1} N_t r_0^2 \sin 2\varphi_0 \cdot \dot{\varphi}_0}{r_m^2 \cos^3 \varphi_n}$	20
III	$2 \times 10^{-2} \frac{\partial N_t}{\partial x} \frac{R_m}{\cos^2 \varphi_m} \cdot \dot{\varphi}_0$	3
IV	$2 \times 10^{-2} \frac{\partial N_t}{\partial y} \frac{R_m}{R_c} \frac{\dot{y}_c}{\cos \varphi_m}$	3
V	$\frac{5.5 \times 10^{-2}}{\cos \varphi_m} \frac{\partial N_t}{\partial t}$	0.5

Parameter	N_e	N_t	$\frac{\partial N_t}{\partial x}$ $\frac{\partial N_t}{\partial y}$	$\frac{\partial N_t}{\partial t}$	$\dot{y}_c$ $\dot{x}_c$	$\dot{\phi}_0$	R_c, R_m r_m	$\Delta\dot{R}_c$
Unit	10^{12} e/m^3	10^{17} e/m^2	10 GU	10^{17} e/m^2 hr	km/sec	mr/sec	10^3 km	m/sec

III. HORIZONTAL GRADIENTS OF N_t

The concern in this section is to assay the magnitude range and variability of horizontal gradients of N_t. The study is primarily a survey and examination of data in the literature. We have in mind a comparison of the observed gradient levels with that given in Table 3. A level of 10 GU and greater means that the refraction will exceed Minitrack precision for satellite altitude above 700 km at the zenith.

Observational Methods. Historically, N_t was first measured from observations on the Faraday rotation in lunar radar experiments (Refs. 23, 24). With the advent of space exploration this technique has been largely superceded by observation on radio beacon signals of earth satellites. The common methods are to observe the Faraday rotation or the Doppler shifted frequency of the transmitted signals. To resolve an ambiguity in the determination of N_t, the preferred procedure in these methods is to employ two harmonically related frequencies, or a pair of closely spaced frequencies. The signal observations then give the integrated electron content along the moving ray path. For satellite altitudes above the ionosphere the data yield essentially N_t corresponding to the sub-ionospheric points of the ray path. The horizontal gradients thereby obtained will be important in our study.

For a series of satellite passages, data on N_t can be acquired at different local times and covering a geographic area about the site. In a limited period of observation there is little secular change in the ionosphere and one determines a distribution function for N_t. Some investigators represent their data as a composite in contours of constant N_t in a plot of latitude vs local time. There is a tacit assumption that the diurnal pattern of N_t in the region of observation is independent of longitude. With this limitation, one can then use the plot to recover mean latitudinal and longitudinal gradients as a function of local time and latitude.

The mean latitudinal gradient between latitudes λ_1 and λ_2 can be determined from the relation

$$\text{lat. grad.} = \frac{N_t(\lambda_2) - N_t(\lambda_1)}{r_m(\lambda_2 - \lambda_1)} . \qquad (37)$$

or,

$$\text{lat. grad. (G.U.)} = \frac{8.5\,(N_t(\lambda_2) - N_t(\lambda_1))}{\lambda_2 - \lambda_1} \tag{38}$$

where N_t/λ is in units of 10^{16} e/m^2 deg.

A longitudinal gradient of N_t can be calculated from the dependence of N_t on local time. The gradient is then given by

$$\text{long. grad.} = \frac{T}{2\pi r_m \cos\lambda} \frac{N_t(t_2) - N_t(t_1)}{t_2 - t_1} \tag{39}$$

where T is the period of rotation of the earth; or

$$\text{long. grad. (G.U.)} = \frac{5.6}{\cos\lambda} \cdot \frac{N_t(t_2) - N_t(t_1)}{t_2 - t_1} \tag{40}$$

where N_t/t is expressed in units of 10^{17} e/m^2 hr. We note however that, contrary to the assumption stated above, the diurnal pattern is dependent on longitude. The ionosphere has consequently an asymmetry which contributes a bias to the long. grad. This effect is smoothed out in the composite data.

Observations on the signals of satellites in a geostationary orbit gives a continuous record of the diurnal pattern of N_t at a fixed sub-ionospheric point. One can also use Eq. (40) to derive the long. grad. contributed by the dependence of N_t on local time.

The deficiency in connection with using Eq. (40) implies that the maximum long. grad. will be underestimated. But since the lat. grad. tends to attain higher levels than the long. grad. the former is of more interest to us.

Scale Size of N_t Gradients. The records of Faraday rotations and Doppler shift observations commonly exhibit irregularities which are attributable to variations in the integrated electron content along the changing direction of the ray path. The smoothed record gives regular ionospheric gradients that are representative of geographic variations. The irregular deviations from the smoothed record are evidence of an ionospheric structure, termed in the literature as "large scale irregularities." Both the regular gradients and irregularities are to be examined for their significance to VHF refraction.

The horizontal scale of the irregularities vary from a few kilometers to many hundreds of kilometers (Ref. 25). The vertical dimension is typically about one-fifth of the horizontal extent. Electron densities are observed to deviate from the mean background by anywhere from several percent to a small fraction of a percent.

There is a minimum size to the irregularities for which the application of refraction theory (Fermat's principle) is admissable. The scale size, L, of the irregular region must be greater than the first Fresnel zone. If R_1 and R_2 are distances of the irregularity from the satellite and ground observer, respectively, and λ is the wavelength of the signal then

$$L > \sqrt{\frac{2 R_1 R_2 \lambda}{R_1 + R_2}}$$

Taking $R_1 = R_2 = 400$ km and λ(VHF) = 2m, then $L > 1$ km, which is about the minimum size associated with large scale irregularities.

Regular Gradients

Equatorial Region. A few determinations of the latitudinal dependence of N_t were made by Olatunji (Ref. 26) from Faraday rotation records during the passages of Transit 4A and 4B for the period May 1962 to January 1963. The station location was Abadan (3.9 °E, 7.5 °N, Magnetic latitude 3 °S). The pre-dawn observations (Fig. 10a) show the lat. grad. is nil (< 1 G. U.), but for the morning hours a maximum of N_t (Fig. 10b) prevails at 8° to 9°N latitude with steep gradients of 5 to 25 G. U. to the north and south of the geomagnetic equator. The morning maximum of N_t gives way to an afternoon depression in N_t (Fig. 10c) with lat. grad. high of 25 to 35 G. U. We mention that the approximate asymmetry of the minimum near the geomagnetic equator is akin to the "equatorial anomaly," wherein the latitudinal dependence of N_{max} (the maximum of the vertical N_e profile) also exhibit a minimum near the geomagnetic equator. At midnight the latitudinal variation of N_t is reverting (Fig. 10c) to a pre-dawn like profile, but the lat. grad. remains appreciable, as high as 6 to 20 G. U.

Tyagi (Ref. 27) measured N_t from the satellite S-66 for a period during the minimum of the sunspot cycle, Oct. 1964 to Sept. 1966. The receiving station at Delhi (28.63 °N, 77.22 °E) recorded data over a wide latitude range. The daytime observations (Fig. 11) covering the geographic latitudes 10 °N to 10 °S

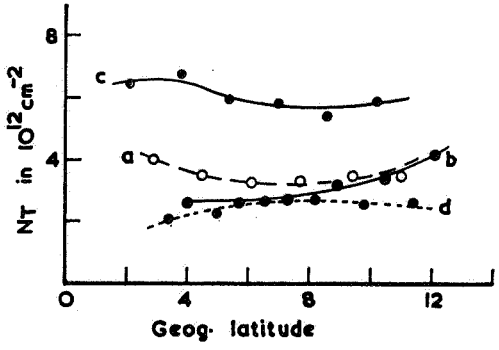

Figure 10(a)—Latitude variation of N_T: 0230-0630 L.M.T. [From Olatunji, Ref. 26].

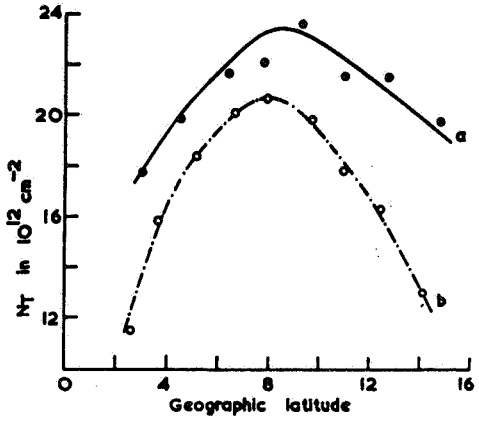

Figure 10(b)—Latitude variation of N_T: 0700-1000 L.M.T. [From Olatunji, Ref. 26].

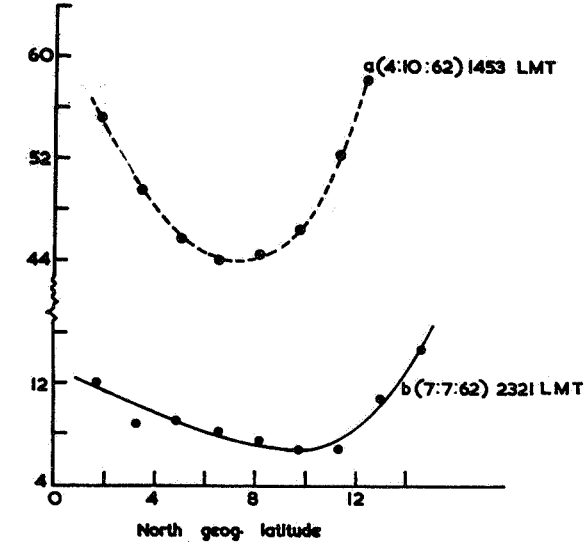

Figure 10(c)—Latitude variation of N_T: 1200-2300 L.M.T. [From Olatunji, Ref. 26].

show lat. grad. of 2 to 20 G. U. The nighttime observations covered the latitude interval 16 °N to 40 °N. The lat. grad. were low, $\lesssim$ 1 G. U. due to the low level of N_t at night. (The logarithmic gradients of N_t in units of inverse degrees are shown in parentheses in Fig. 11.) Tyagi also gives a summary on the diurnal variation of N_t. These data imply a long. grad., $\sim$ 3 G. U. for daylight hours during the equinox.

Observations on N_t in equatorial region during 1964 (sunspot minimum) were made by Rufenach et al (Ref. 28). The observations of signals of Transit 4-A involved a cooperative effort of ground station at Bangkok, Singapore, and Hong Kong. The long. grad. (deduced from diurnal variations) of N_t were low, about 2 G. U. and less. The data on latitudinal variations of N_t for May-June 1964 (Fig. 12a) and Aug. - Sept. 1964 (Fig. 12b) show large lat. grad. during the late morning and early afternoon of 10 G. U. to 30 G. U., but near the magnetic equator, where N_t is an extremum, the gradients are nil.

Basu et al (Ref. 29) have measured the latitudinal variations of N_t for quiet and disturbed geomagnetic conditions. The data is derived from signals of the beacon satellite S-66 at Calcutta, 23°N (dip 32°N). The observations on quiet days exhibit an interesting regularity (Fig. 13a). The curves of N_t all peak around 23° north latitude and decrease toward both the geomagnetic equator and higher latitudes. The influence of seasonal effects and solar

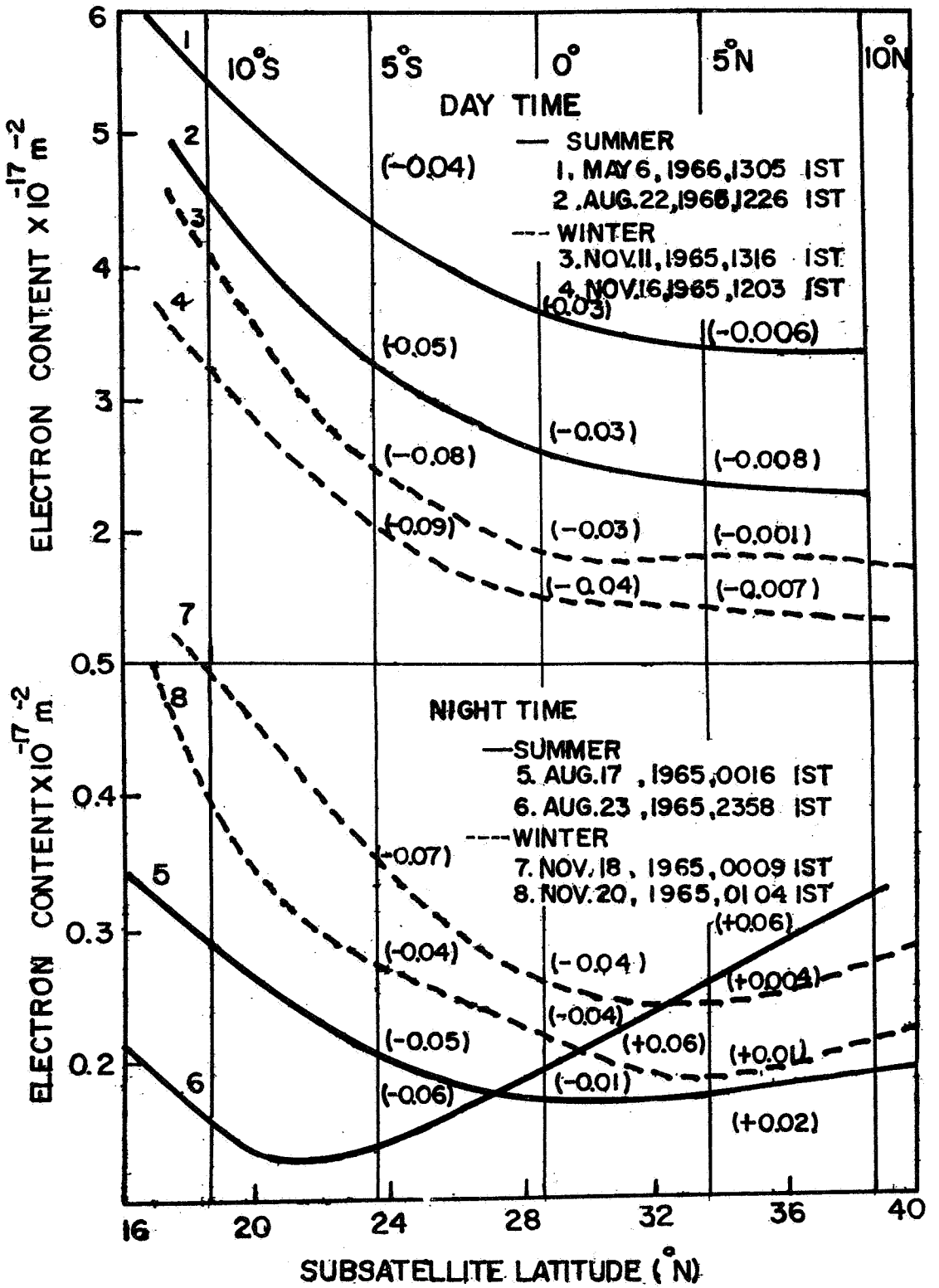

Figure 11—Latitudinal dependence of N_t. [From Tyagi, Ref. 27].

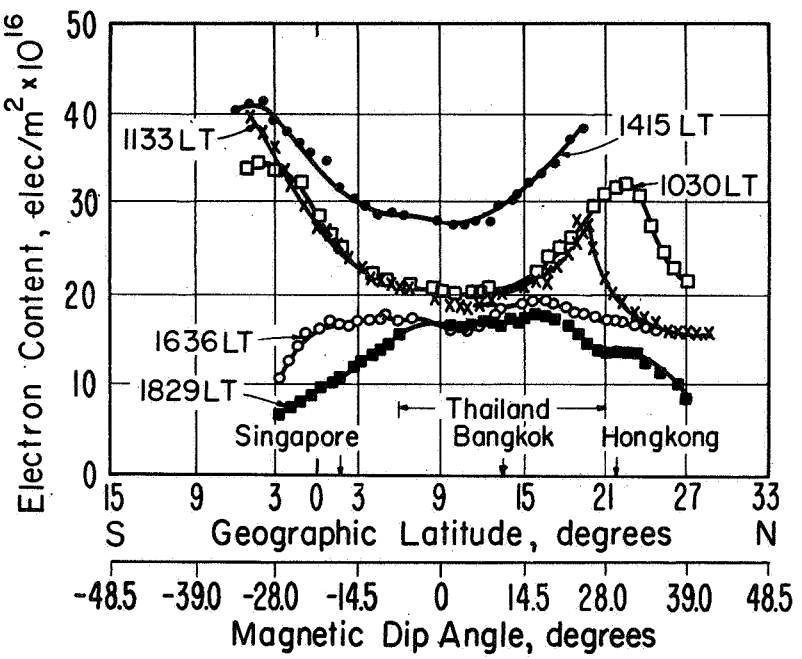

Figure 12(a)—Latitudinal variation of electron content: three-station analysis for May and June 1964. [Rufenach, et al., Ref. 28].

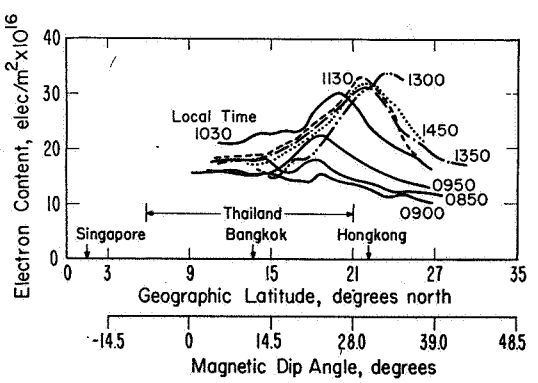

Figure 12(b)—Latitudinal variation of electron content: two-station analysis for August and September 1964. [From Rufenach, et al., Ref. 28].

activity appears as a relative displacement of the curves and a systematic change in slope. Toward the magnetic equator the observed slopes are 25 to 50 G. U. Fig. 13b compares the noontime latitudinal variation of N_t for magnetically quiet and disturbed days. The significant changes during disturbed days is a decrease and flattening of the slope toward the lower latitudes, while at higher latitudes the lat. grad. are general high, about 20 to 50 G. U.

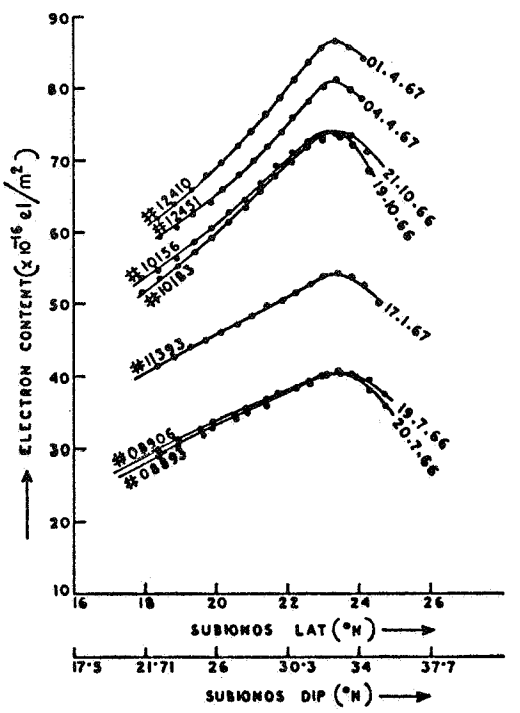

Figure 13(a)—Variation of electron content with latitude under magnetically quiet conditions in different seasons. [From Basu, et al, Ref. 29].

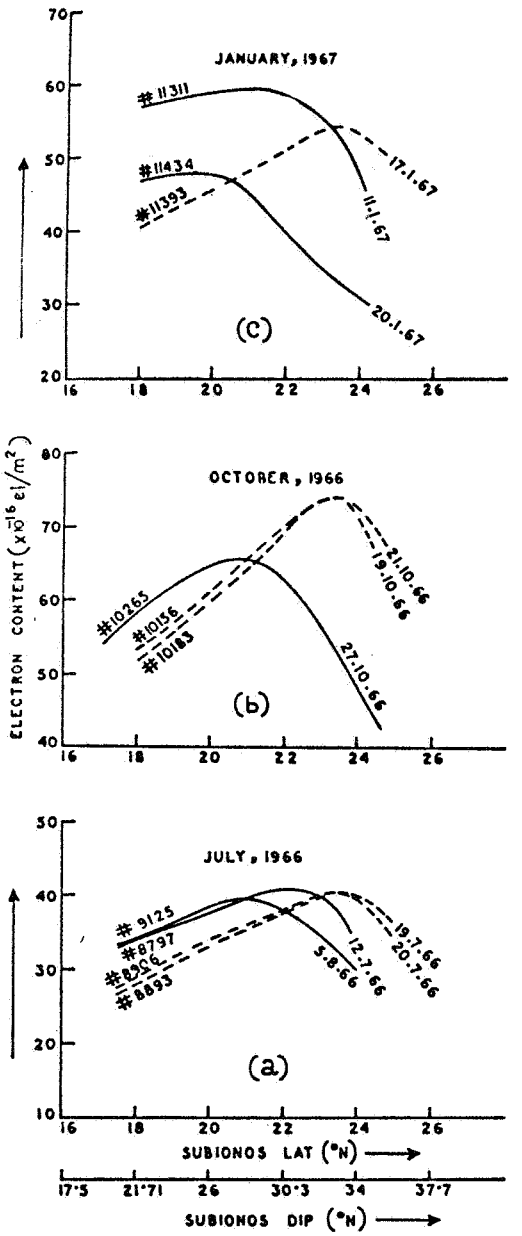

Figure 13(b)—Comparison of latitude variation of electron content under magnetically quiet and active conditions in (a) summer (July 1966), (b) fall (October 1966), and (c) winter (January 1967). The solid line curves represent active conditions, and broken line curves represent quiet conditions. [From Basu, et al, Ref. 29].

The diurnal variations of N_t (Fig. 1a, b, c) observed by Garriott, et al during the relatively low period of the sunspot cycle, Sept.-Nov. 1964, at Hawaii from signals of Syncom III show a rapid morning rise and evening set (Ref. 1). The day to day variations in these rates are themselves highly variable and correspond to long. grad. of 1 to 6 G. U. The long. grad. during the night are nil. Coordinates of the sub-ionospheric point are 19.7°N, 159.8°W.

Mid-latitude Region. de Mendonca (Ref. 30) calculated N_t from measurements of the differential Doppler frequency shift of Transit 2-A. Observations were made at Stanford University during the months July-Oct. 1960, a period of high solar activity. The determinations of N_t are shown as contours of constant N_t in two plots of geographical latitude vs local time, one for July-Aug. 1960 (Fig. 14a) and the second for Sept.-Oct. 1960 (Fig. 14b). The difference in the data of the two figures for their common time interval 1200 to 1600 LT is due to the seasonal change in the ionosphere between the periods. The long. grad. and lat. grad. are determined as prescribed by Eqs. (38, 40). The gradients are seen to vary over a wide range of magnitude and direction. During midday the direction is predominantly latitudinal and during the pre-dawn and post-sunset hours predominantly longitudinal.

For the period July-Aug. 1960 the midday lat. grad. varies from about 8 to 40 G. U. An inspection of the long. grad. at the 30° latitude indicates about 8 G. U. at sunset and 6 G. U. at sunrise. During most of the daylight hours the gradients of N_t are from 5 to 10 G.U., but at night the level drops to 1 to 2 G. U. and less.

In the period Sept.-Oct. 1960, the midday level of N_t is about 50% higher than during the preceding summer months. The midday lat. grad. is uniformly high at about 20 G. U. The gradients after sunset also have a relatively high long. grad. of 5 to 10 G. U.

The Joint Satellite Studies Group (Ref. 31) made observations on N_t in the European sector during October 1963 and during October 1964. The data was reduced from Faraday rotations of signals from Transit 4A and Explorer 22. The program examined geographical distribution of electron content under differing geomagnetic conditions. A unique feature of this effort was simultaneous measurement of N_t from several tracking stations. An example given in Fig. 15a shows electron content variations along three sub-ionospheric traces. The Studies Group utilized this type data and other ionospheric sounding data to construct tridimensional (relief) representations showing electron content as a function of geographical location. Two such representations for differing geomagnetic conditions are shown: Fig. 15b, for the quiet magnetic state has gradients of about 10 G. U. radiating from an area of minimum N_t ; Fig. 15c, for the disturbed magnetic state has gradients of 10 to 20 G. U. having a north-east to south-west orientation. These are relatively high gradients for a period of near minimum solar activity.

Determination of the latitude dependence of N_t have been made by Weise and Yeh (Ref. 32) at the University of Illinois for the period Oct. 1964 to March 1965. Observations were made of the Faraday effect on signals of Explorer 22. The horizontal gradients of N_t were consistently very low $\leq$ 2 G. U.

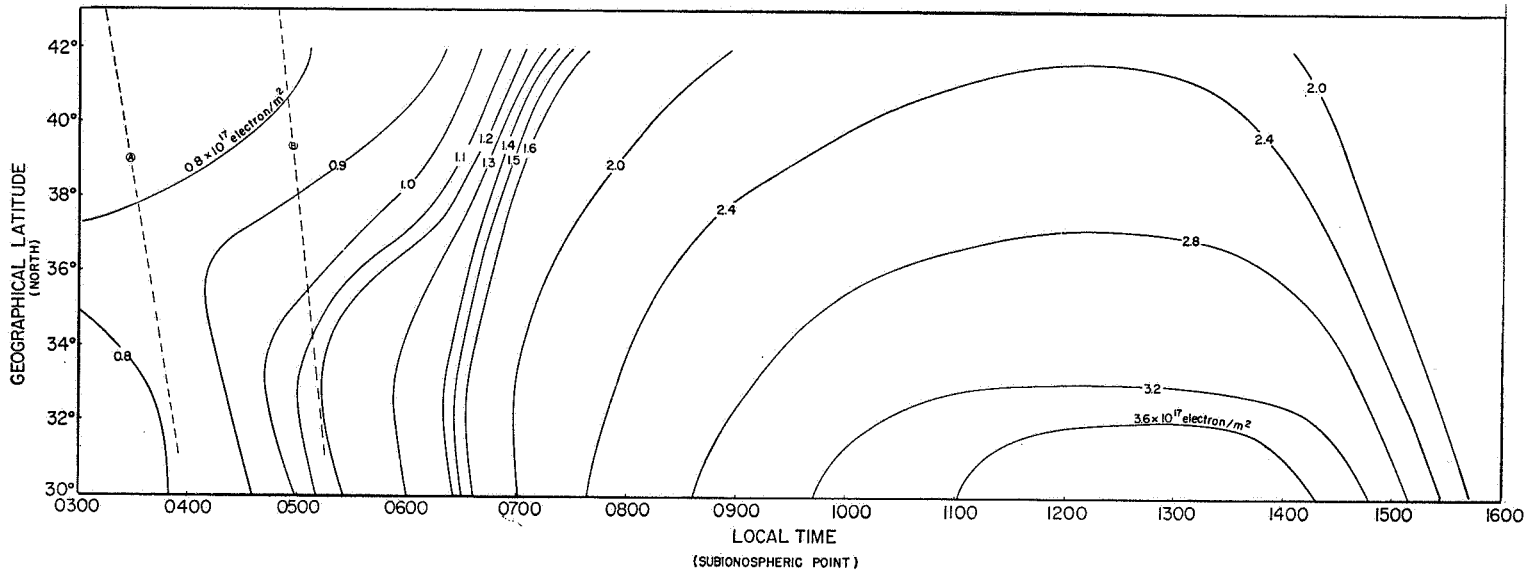

Figure 14(a)—Smoothed curves of constant $\int N\,dh$ derived from measurements on quiet days during July and August 1960. Curve A represents sunrise at sea level and curve B sunrise at height h = 400 km for July 29, 1960. [From de Mendonca, Ref. 30].

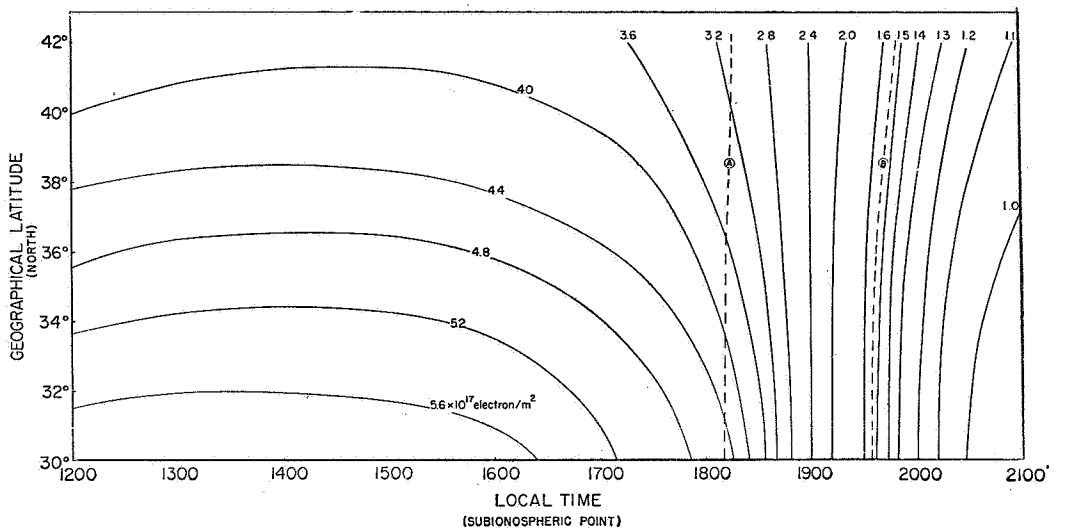

Figure 14(b)—Smoothed curves of constant $\int N\,dh$ derived from measurements on quiet days during September and October 1960. Curve A represents sunset at sea level and curve B sunset at height h = 400 km for September 12, 1960. [From de Mendonca, Ref. 30].

Auroral Region. Liszka (Ref. 34) determined N_t at Kiruna, Sweden (67.8°N, 20.3°E) from signals of the satellite S-66. His observation covers the period, Nov. 1964 and the Winter 1964-65. Detailed records of N_t for a series of satellite passes during Nov. 1964 show lat. grad. of 2 G. U. before local noon and after midnight. A representation of observations during the winter are shown in a plot of local time vs geographic latitude (Fig. 16). The observed data were within ±1 hour of the Kiruna meridian. The diurnal cycle is covered for the latitudes 55°N to 72°N. The notable feature in the contours of constant N_t is the existence of the minimum which dominates the pattern in the nighttime over an extended latitude interval. During the morning hours (~ 0700 to 1100 l. t.) the gradients are predominantly longitudinal, about 1 to 3 G. U. in magnitude. In

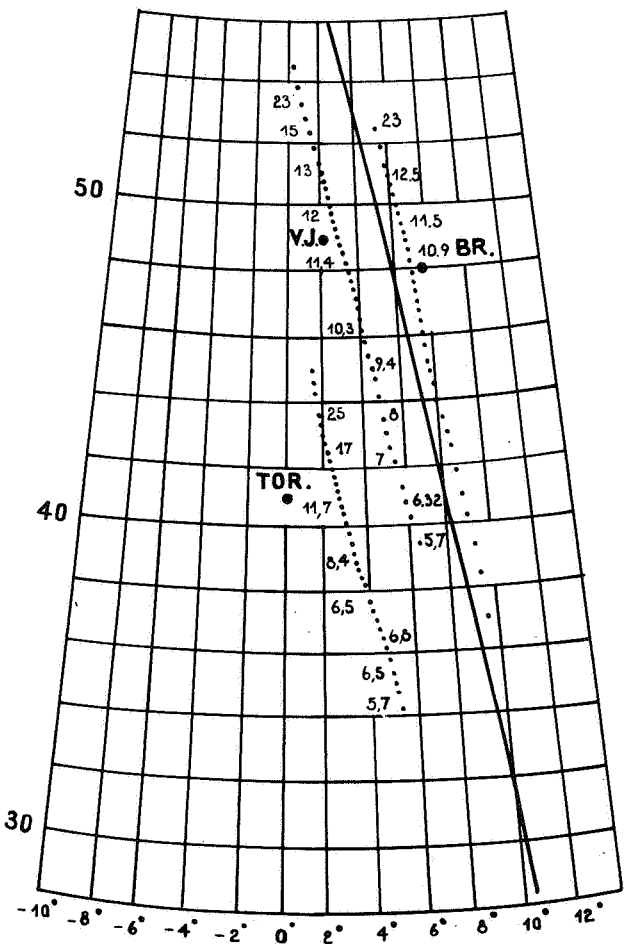

Satellite : Explorer 22
Rev. 118
Date 18.10.64
Z = 17 h
K = 2

Figure 15(a)—Tracing of the sun-ionospheric lines in terms of the geographical latitude and longitude; the figures give the total electron content in 10^{16} e/m^2. [From Bertin, et al., Ref. 31].

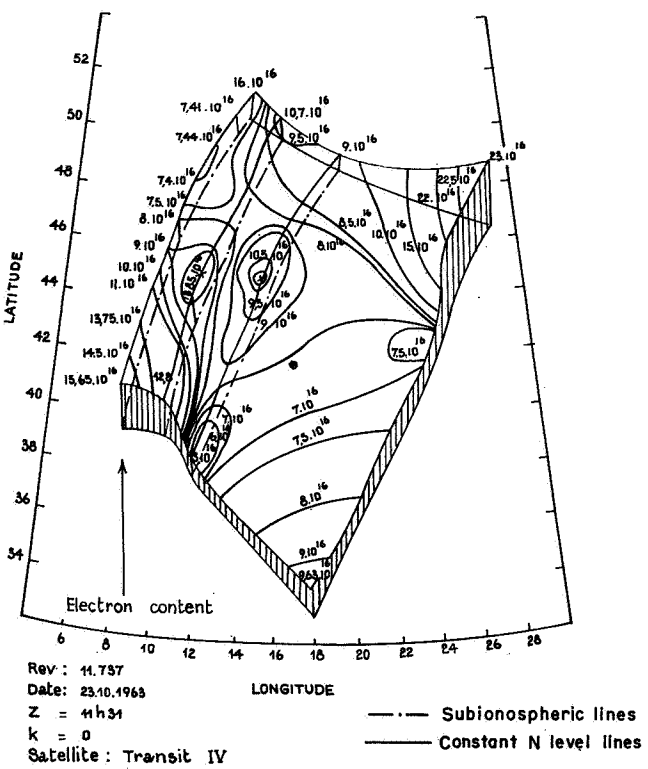

Figure 15(b)—Tridimensional representation of the distribution of the total electron content in 10^{16} el/m^2. [From Bertin, et al., Ref. 31].

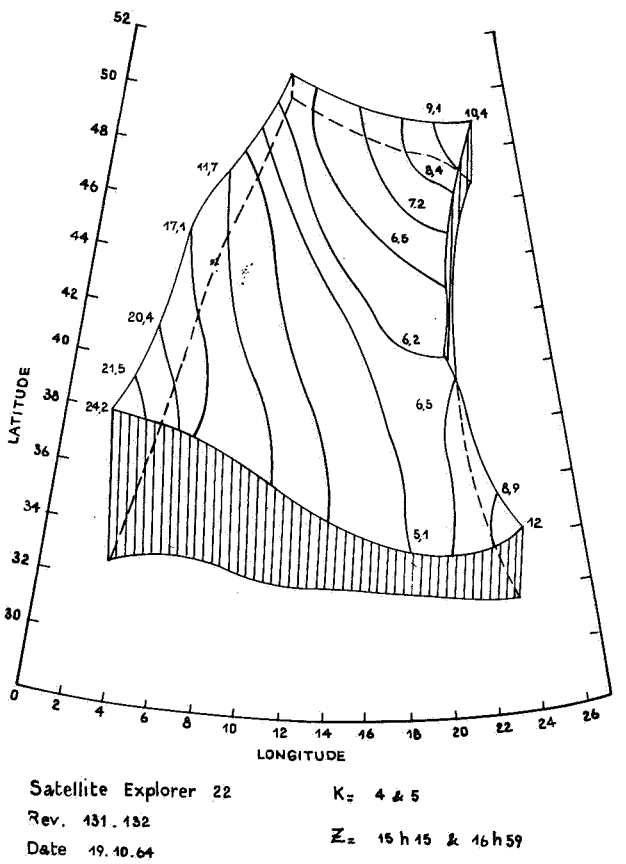

Figure 15(c)—Tridimensional representation of the distribution of the total electron content in 10^{16} el/m^2. [From Bertin, et al., Ref. 31].

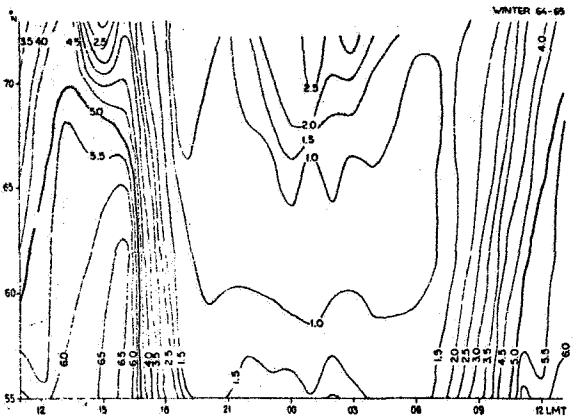

Figure 16—Latitidunal and diurnal variations of the ionospheric electron content near the auroral zone during winter 1964-65. Units are 10^{16} e/m^2. [From Liszka, Ref. 34].

the late afternoon from 1200 to 1700 l. t. the pattern is irregular with gradients of 1 to 5 G. U. The low level of gradients is due to the very low range of N_t ($\lesssim 5 \times 10^{16}$) and characteristic of the minimum in the solar cycle. On the otherhand, the logarithmic derivative of N_t is large, so that during the more active phase of the solar cycle one would look for an appreciably higher gradient of N_t.

Rai and Hook (Ref. 33) measured the latitudinal dependence at N_t at College, Alaska during the winter 1963-64. The signals were from satellite 1963-38c. The gradients had a generally low level of about 3 G. U. and less. This again corresponded to the low level of N_t which was $\lesssim 1 \times 10^{17}$ e/m^2.

Large Scale Irregularities of N_t.

Mid-latitude Region. Merrill et al (Ref. 35) analyzed irregularities in the Faraday rotation records of the 20 mHz signal of Sputnik. The observations were

made at Boulder for the period Sept. 1958 to March 1960. This was an epoch of high solar activity for which the integrated electron content N_t had a diurnal range from a nighttime minimum of 1×10^{17} e/m^2 to a midday maximum of 9×10^{17} e/m^2 (Ref. 36). The horizontal dimensions of the observed irregularities were typically about 150 km to 200 km. The excursion within the irregularities from the mean background of N_t was about 1% to 2.5%. Their gradients in the nighttime were about 1 G. U. and the mean for the daytime was 3 G. U., while the midday maximum was 6 G. U.

Titheridge (Ref. 25) analyzed the Faraday fading records of the 20 mHz transmissions of Explorer for the period Nov. 1960 to Aug. 1961. The location was near Auckland, New Zealand (lat. 30.01°S, long. 174.98°E). Some 700 irregularities was observed varying in horizontal extension from 5 km to 500 km. The data, summarized in Fig. 17, gives the gradients (c/s ≡ 1 G. U.) vs local time. The "a" plot is for summer and the "b" plot for winter. In general the gradients are very low, less than 1.0 G. U. It should be noted that the level of N_t was very low. The midday peak is 2.5×10^{17} e/m^2 in the summer and 1.5×10^{17} e/m^2 in the winter months.

Roger (Ref. 37) deduced gradients of large scale irregularities from observations on the 108 mHz signal of Vanguard at Jodrell Banks. The period was Nov. 1959 to Feb. 1960 and July-Aug. 1960. His data show average gradients of 2.5 G. U. The observations of Merrill, et al, and Roger made at similar times in mid-latitude regions agree on the level of the gradients.

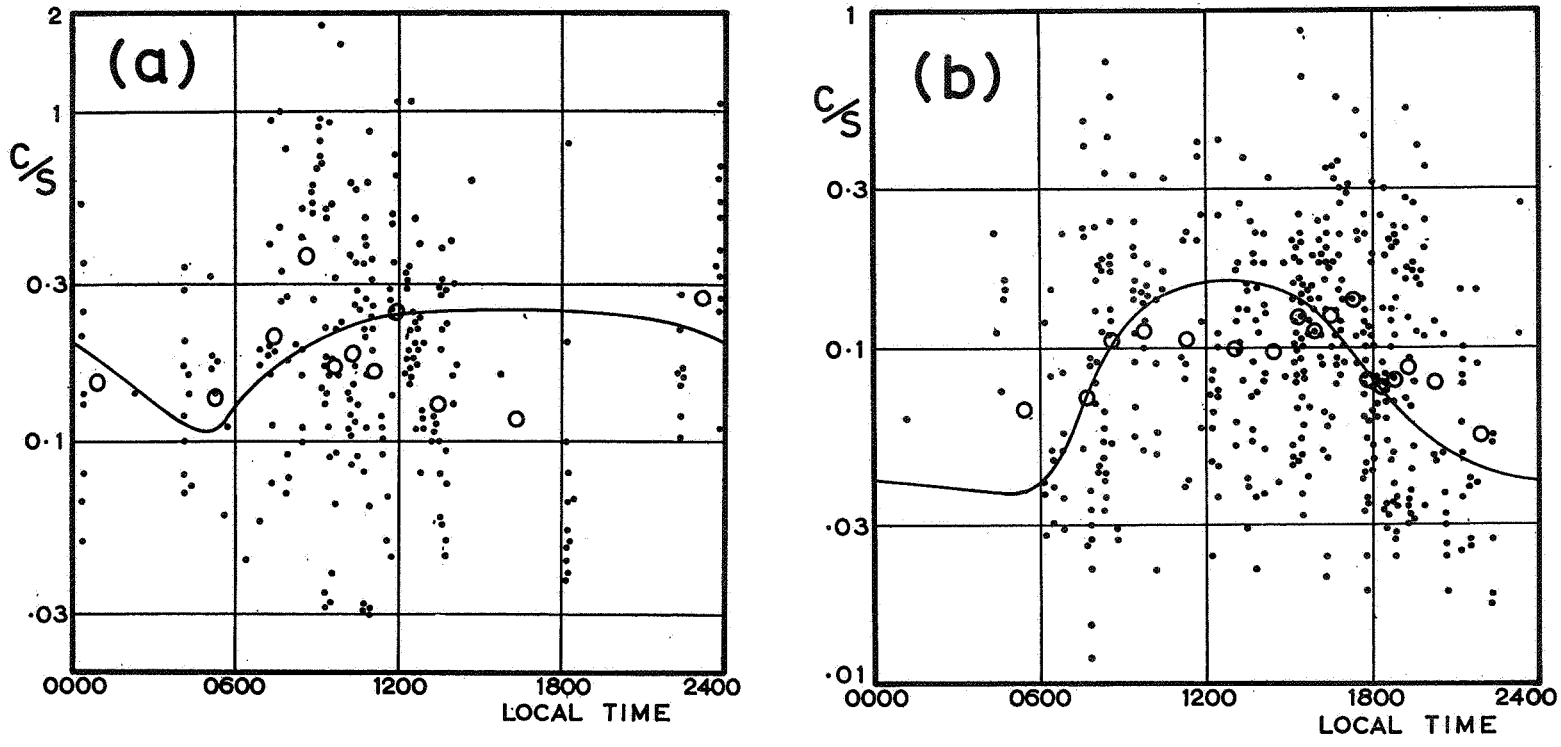

Figure 17—The ratio of the content (C) in 10^{14} electrons/m^2 to the size (S) in kilometers. The continuous lines are proportional to the total electron content of the ionosphere. The circles show the variation in the mean value of C/S. (a) Summer; (b) Winter. [From Titheridge, Ref. 25].

Bhonsle (Ref. 38) obtained data on gradients of irregularities for a period of low solar activity, Oct. 1964 to Oct. 1965. The deductions are based on the Doppler shift of beacon signals of S-66. The stations was at Stanford. The average gradient was 1 G. U.

IV. CONCLUDING REMARKS

Horizontal Gradients of N_t.

Observational data on the regular gradients of N_t have wide variations that show, like N_t, the influence of time of day, geographical location, phase of the sunspot cycle, and geomagnetic disturbances. The largest gradients of N_t prevail during daylight hours and have predominantly a latitudinal direction The general trend of the midday latitudinal profile of N_t is an irregular decrease from the equatorial region to the auroral regions. A common feature of this pattern is a depression of N_t at the geomagnetic equator.

During the period of lowest sunspot number the latitudinal gradients in the equatorial region may attain a level as high as 10 G. U. and during the phase of high solar activity 60 G. U. has been observed. For the mid-latitude region the observational data indicate latitudinal gradients approaching the levels of the equatorial region, At sunrise and sunset, gradients are predominantly longitudinally directed, and attaining levels of 10 G. U. for the solar maximum.

In the near auroral region the limited observational data show gradients of several G. U. during a period of low sunspot number. The region however has strong

irregularities and correspondingly large logarithmic gradients of N_t. For high sunspot number the gradients might attain a more significant level.

The gradients of N_t stemming from large scale irregularities are substantially less, by about an order of magnitude, than those of regular gradients and show the influence of sunspot number. Most observations on the irregularities have been confined to the mid-latitude region. During high sunspot number, gradients are typically 2.6 G. U. during the day with a maximum of about 6 G. U., while at lower sunspot number the magnitudes are generally negligible.

Refraction

The effects of a three dimensionally heterogeneous ionosphere on refraction formulas is to add to the known terms of a spherically layered medium other terms with horizontal gradients. The familiar terms (associated with spherical symmetry) attain the largest magnitude, but they also vanish at points of symmetry, namely at the zenith for refraction and at the satellite point-of-closest approach in range-rate tracking. On the tracking interval where these terms are accordingly minimal, the horizontal gradients of the ionosphere distinctively can contribute a predominant effect, sufficient to warrant consideration in the analysis of tracking data. For Minitrack, we also mention that at relatively large zenith angles (say, 45°) and large range (several earth radii) the refraction terms of horizontal gradients in N_t cannot only exceed the limits of instrumental precision, but can as well attain a general level of comparability with the term, $d\varphi_0^{(1)}$.

The latter remark on Minitrack should be qualified because instrumental error is a function of signal strength. The radiation level of satellite signals is of course power limited. Then for a fixed power level there is a range beyond which instrumental errors must increase. Tracking precision can deteriorate rapidly with increased satellite range (Ref. 39). This effect eventually overwhelms ionospheric perturbation. As radiated power levels of a small fraction of a watt suffice for near earth orbit it would appear that an increased power level is possible, thus extending the high precision to a range of an earth radius and more. It is in this eventuality that refraction due to horizontal gradients is particularly relevant to Minitrack.

Ionospheric Monitoring and Modeling

We have in the main body of this report given a framework for the analysis of ionospheric perturbation on VHF tracking and used observational data to study the magnitude and variability of the perturbations. In order though to apply the analysis to tracking data, a description of the ionospheric state is needed corresponding to the time and site of the tracking. But the wide and irregular variability of the ionosphere dictate that some monitoring of the medium be conducted in conjunction with the tracking events. We will describe in rudimentary form a method for such ionospheric monitoring and modeling. This method, to be outlined in the immediate following paragraphs, raises questions concerning errors associated with the model or concerning tracking requirements satisfied by the method. These are rather ramified matters. A close statement here is

hardly possible. Abundant observational data over extended periods and experience with the method are likely to be best guides to answer the questions.

The method we have in mind is one giving a description of spatial and temporal variations of the three dimensionally inhomogeneous ionosphere for the individual STADAN sites. A local vertical profile N_e (h) is to be constructed from observed bottomside profile $N_{e,b}$ (h) and a calculated topside profile $N_{e,a}$(h). A model of horizontal gradients in this profile then complete the three dimensional structures.

The monitor makes two types of standard ionospheric observations in the neighborhood of each tracking site. One set of observations in on the bottomside profile. The other set is on N_t. The feasibility of the later observation is predicated on the expectation that there will in the near future be within the view of each site a geostationary satellite whose signals can be utilized for monitoring N_t. The increased applications role of these satellites makes the expectation appear to be a reasonable one.

With these observations a complete vertical profile is constructed as follows. The $N_{e,b}$(h) gives N_{max}, h_{max}, and the bottomside electron content N_b by the formula

$$N_b = \int_0^{h_{max}} N_{e,b}\,(h)\,dh \qquad (42)$$

For the topside, we assume a model of constant scale parameter, H_a, for the Chapman profile

$$N_{a,e} = N_{max} \exp \frac{1}{2} \left\{ 1 - \frac{h - h_{max}}{2H_a} - e^{-\frac{h-h_{max}}{2H_a}} \right\} \tag{43}$$

Although the parameter H_a is known to be a function of altitude, the profile can be adequately described for the purposes of a refraction model by a constant, independent of height.

The topside electron content N_a is given by the integral

$$N_a = \int_{h_{max}}^{\infty} N_{e,a}(h)\, dh \tag{44}$$

For the Chapman model (Ref. 40)

$$N_a = 2.13\, H_a\, N_{max} \tag{45}$$

Then the relation

$$N_t = N_a + N_b \tag{46}$$

combined with Eq. (45) gives the topside parameter H_a. Thus a vertical profile is determined for one location in the site area.

Note that the bottomside profile and N_t which form the bases for determining the complete profile, will generally be observed at geographical points having a finite separation. In the construction of $N_e(h)$ there was the tacit assumption that the observations can be identified with a common location. This involves an assumption on horizontal gradients, to be considered next.

The desired circumstance for monitoring horizontal gradients in the neighborhood of a given site is to have observations on $N_{e,b}$ (h) and N_t from pairs of stations having an appropriate latitudinal and longitudinal separation. Where this is not the case we must look to other means.

The latitudinal gradients can be relatively large hence their determination requires care. A fortunate feature is the location of a number of STADAN sites and ionospheric stations near the 75°W meridian. This is favorable for cooperative observation and determination of latitudinal gradient. The other STADAN sites can be expected to present unique problems according to the disposition (or lack thereof) of observing stations in their region.

Of particular interest for the study of latitudinal gradients are the polar orbiting topside sounders. The data already obtained provides a considerable basis for developing a model on latitudinal gradients.

For longitudinal gradients, where stations are not suitable located, there are other means as well. As previously stated longitudinal gradients can be attributed to the diurnal process and asymmetry in the ionospheric (or geomagnetic) field. The part of the longitudinal gradient due to the diurnal effect can be determined from the local measurement of the pattern as given by Eq. (40). To determine the contribution of this asymmetry, the global data in Ionospheric Predictions, published monthly by ESSA would be a source of data worth studying.

The effectiveness with which the general scheme of model and monitoring the ionosphere as just described can be used in analysis of ionospheric perturbation is enhanced by the direct observations on N_t which is the central parameter. A limitation on the model rests with uncertainty in the determination of horizontal gradient of N_t.

APPENDIX A

Refraction in a Heterogeneous Ionospheric Medium*

Writing the line element ds in the Fermat principle as

$$ds = \sqrt{dx^2 + dy^2 + dz^2} \tag{A1}$$

or since $r = r_o + z$ and $dx = r d\theta$

$$ds = \sqrt{1 + \left(r \frac{d\theta}{dr}\right)^2 + \left(\frac{dy}{dr}\right)^2}\, dr \tag{A2}$$

one derives from Eq. (16) the familiar Lagrangian equations

$$\frac{d}{dr}\left\{\frac{\mu r^2 \frac{d\theta}{dr}}{\sqrt{1 + \left(r \frac{d\theta}{dr}\right)^2 + \left(\frac{dy}{dr}\right)^2}}\right\} - \sqrt{1 + \left(r \frac{d\theta}{dr}\right)^2 + \left(\frac{dy}{dr}\right)^2}\, \frac{\partial \mu}{\partial \theta} = 0 \tag{A3}$$

$$\frac{d}{dr}\left\{\frac{\mu \frac{dy}{dr}}{\sqrt{1 + \left(r \frac{d\theta}{dr}\right)^2 + \left(\frac{dy}{dr}\right)^2}}\right\} - \sqrt{1 + \left(r \frac{d\theta}{dr}\right)^2 + \left(\frac{dy}{dr}\right)^2}\, \frac{\partial \mu}{\partial y} = 0 \tag{A4}$$

*The analysis of this appendix follows closely that of Al'pert (Ref. 14).

Multiplying by dr and integrating we have, using Eqs. (9) and (A2)

$$\frac{\mu r \sin\phi}{\sqrt{1+\left(\frac{dy}{dr}\right)^2 \cos^2\phi}} - \left(\frac{\mu r \sin\phi}{\sqrt{1+\left(\frac{dy}{dr}\right)^2 \cos^2\phi}}\right)_0 = \int_0^s \frac{\partial\mu}{\partial\theta} ds \qquad (A5)$$

$$\mu \frac{dy}{ds} - \left(\mu \frac{dy}{ds}\right)_0 = \int_0^s \frac{\partial\mu}{\partial y} ds \qquad (A6)$$

When $\partial\mu/\partial\theta = 0$, Eq. (A5) becomes Snell's law for spherical symmetry, viz.,

$$\mu r \sin\phi - (\mu r \sin\phi)_0 = 0 \qquad (A7)$$

For

$$\frac{\partial\mu}{\partial y} = 0,$$

$$\mu \frac{dy}{ds} - \left(\mu \frac{dy}{ds}\right)_0 = 0 \qquad (A8)$$

and the ray path is confined to the plane of incidence.

The refraction will be calculated under the condition of Eqs. (17a, b and c); that is,

$$d\phi \ll 1 \qquad (A9)$$

$$d\alpha \ll 1 \qquad (A10)$$

Eq. (A5) can be written to terms in first order as

$$\mu\, r \sin\phi - (\mu\, r \sin\phi)_0 = \int_0^s \frac{\partial \mu}{\partial \theta} ds = -\eta \int_0^s \frac{\partial N_e}{\partial \theta}\, ds \tag{A11}$$

since $dy/ds \doteq d\alpha \ll 1$ and where we have the relation for the refractivity

$$\mu - 1 = N_i = -\eta N_e \tag{A12}$$

From Eqs. (A11) and (9) we have

$$r \frac{d\theta}{dr} = \tan\phi = \frac{r_0 \sin\phi_n - \eta \int_0^s \frac{\partial N_e}{\partial \theta}\, ds}{\sqrt{\mu^2 r^2 - \left(r_0 \sin\phi_n - \eta \int_0^s \frac{\partial N_e}{\partial \theta}\, ds \right)^2}} \tag{A12}$$

where the refractivity at $r = r_0$ is taken to be zero and the refracted angle ϕ at o is ϕ_n.

Using Eq. (13), we have to terms of the first order under the approximations (17) and (A9) that

$$r \frac{d\theta}{dr} = \frac{r_0 \sin\phi_0}{\Omega(r)} + \frac{\delta\phi_0\, r_0\, r^2 \cos\phi_0}{\Omega^3(r)} + \frac{\eta N_e\, r_0\, r^2 \sin\phi_0}{\Omega^3(r)}$$

$$- \frac{\eta r^2}{\Omega^3(r)} \int_0^s \frac{\partial N_e}{\partial \theta}\, ds \tag{A13}$$

where

$$\Omega(r) \equiv \sqrt{r^2 - r_0^2 \sin^2 \phi_0} \tag{A14}$$

Now multiplying by dr/r and integrating from o to c, we get

$$\int_0^{\theta_c} d\theta = r_0 \sin \phi_0 \int_{r_0}^{r_c} \frac{dr}{r\,\Omega(r)} + r_0 \cos \phi_0 \, d\phi_0 \int_{r_0}^{c} \frac{r dr}{\Omega^3(r)}$$

$$+ \eta\, r_0 \sin \phi_0 \int_{r_0}^{r_c} \frac{N_e\, r dr}{\Omega^3(r)} - \eta \int_{r_0}^{r_c} \frac{r dr}{\Omega^3(r)} \int_0^s \frac{\partial N_e}{\partial \theta}\, ds \tag{A15}$$

As the path of integration can to first approximation be taken along the line-of-sight, we obtain from Eqs. (8), (9), and (A14) that

$$\int_0^{\theta_c} d\theta = \int_{r_0}^{r_c} \frac{r_0 \sin \phi_0\, dr}{r\,\Omega(r)} \tag{A16}$$

and

$$\Omega(r) = r \cos \phi \tag{A17}$$

Hence the first term on the right side of Eq. (A15) cancels the left side giving for the refraction

$$d\phi = \frac{-\eta \tan\phi_0 \int_{r_0}^{r_c} \frac{N_e\, r\,dr}{\Omega^3(r)} + \frac{\eta}{r_0 \cos\phi_0} \int_{r_0}^{r_c} \frac{r\,dr}{\Omega^3(r)} \left(\int_0^R \frac{\partial N}{\partial \theta}\, dR \right)}{\int_{r_0}^{r_c} \frac{r\,dr}{\Omega^3(r)}} \tag{A18}$$

where dR, the rectilinear line element, has replaced ds.

The denominator of (A18) is evaluated using Eq. (A14),

$$\int_{r_0}^{r_c} \frac{dr}{r^2 \cos^3\phi} = \int_{r_0}^{r_c} \frac{r\,dr}{(r^2 - r_0^2 \sin^2\phi_0)^{3/2}} = (r_0 \cos\phi_0)^{-1} - (r_c \cos\phi_c)^{-1} \tag{A19}$$

The second term in the numerator of Eq. (A18) may be simplified by interchanging the order of integration. Thus

$$\int_{r_0}^{r_c} \frac{dr}{r^2 \cos^3\phi} \left(\int_0^R \frac{\partial N}{\partial \theta}\, dR \right) = \int_0^{R_c} \frac{\partial N}{\partial \theta}\, dR \left(\int_r^{r_c} \frac{dr}{r^2 \cos^3\phi} \right)$$

$$= \int_0^{R_c} dR\, \frac{\partial N}{\partial \theta} \{(r \cos\phi)^{-1} - (r_c \cos\phi_c)^{-1}\} \tag{A20}$$

From the geometry of Fig. 5 we have for the distance R from o along S_0

$$R = r \cos\phi - r_0 \cos\phi_0 \tag{A21}$$

Using Eqs. (7), (8), (A20), (A19), and (A21) one can rewrite Eq. (18) as

$$d\phi_0 = -\frac{\eta\, r_0\, r_c \sin\phi_0 \cos\phi_c}{R_c} \cdot \int_{r_0}^{r_c} \frac{N_e\, dr}{r^2 \cos^3\phi} + \eta \int_0^{R_c} \frac{(R_c - R)}{R_c} \frac{\partial N_e}{\partial x} \frac{dR}{\cos\phi} \quad \text{(A22)}$$

To calculate $d\alpha_0$ we return to Eq. (A6). We mention that Al'pert gives in place of Eq. (A6) a form that is symmetrical with Eq. (A5). Our procedure simplifies the calculation.

Since $d\alpha_0 \doteq (dy/ds)_0$ to first order terms, we have integrating Eq. (A6) from o to c along the line-of-sight

$$\int_{y_0}^{y_c} dy - d\alpha_0 \int_0^{R_c} \frac{dR}{\mu} = \int_0^{R_c} \frac{dR}{\mu} \left(\int_0^{R} \frac{\partial \mu}{\partial y}\, dR \right) \quad \text{(A23)}$$

The first term on left side vanishes since the end-points of ray S are on the plane I. Hence we have, interchanging the order of integration,

$$d\alpha_0 = -\frac{\int_0^{R_c} \frac{\partial \mu}{\partial y}\, dR \left(\int_R^{R_c} \frac{dR}{\mu} \right)}{\int_0^{R_c} \frac{dR}{\mu}} \quad \text{(A24)}$$

Then to first order terms in the refractivity

$$d\alpha_0 = \frac{\eta \int_0^{R_c} \frac{\partial N_e}{\partial y} dR \left(\int_R^{R_c} dR \right)}{\int_0^{R_c} dR} \tag{A25}$$

Finally,

$$d\alpha_0 = \eta \int_0^{R_c} \frac{\partial N_e}{\partial y} \frac{(R_c - R)}{R_c} dR \tag{A26}$$

The formulas in Eqs. (A22) and (A25) for $d\phi_0$ and $d\alpha_0$ are due Mityokova and Mityakova (Ref. 15).

The refraction of the azimuthal angle $d\alpha_0$ is

$$d\alpha_0 = \frac{d\alpha_0}{\sin \phi_0} \tag{A27}$$

In connection with the Doppler effect it is useful to have the refraction angles at the satellite. We have similar to the derivations leading to Eqs. (A21) and (A25) that

$$d\phi_c = + \frac{\eta\, r_0\, r_c \sin\phi_c \cos\phi_0}{R_c} \int_{r_0}^{r_c} \frac{(N_e(\vec{r}) - N_e(\vec{r}_c)\, dr)}{r^2 \cos^3\phi}\, dr$$

$$- \eta \int_0^{R_c} \frac{R}{R_c} \frac{\partial N_e}{\partial x} \frac{dR}{\cos\phi} \qquad \text{(A28)}$$

and

$$d\alpha_c = - \eta \int_0^{R_c} \frac{R}{R_c} \frac{\partial N_e}{\partial y}\, dR \qquad \text{(A29)}$$

REFERENCES

1. GRARR System Design Evaluation Report, prepared by General Dynamics, Contract No. NAS 5-10555, R-67-042, Dec. 13, 1967.

2. Marsh, J. G., G. E. Doll, R. J. Sandifer, and W. A. Taylor, Intercomparison of the Minitrack and Optical Tracking Network Using GEOS-I Long Arc Orbital Solutions, X-552-68-105, GSFC, Dec. 1967.

3. Lerch, F. J., J. G. Marsh, M. D. d'Aria, and R. L. Brooks, GEOS-I Station Tracking Positions on SAO Standard Earth (C-5), X-552-68-70, GSFC, Dec. 1967.

4. Freeman, J. J., Final Report on Ionospheric Correction to Tracking Parameters, NASA Contract NAS5-9782, Nov. 1965.

5. Rosenbaum, B., Compensation of VHF Ionospheric Radar Tracking Effects, Tech. Brief, GSFC, Apr. 1965.

6. I. J. Cole, F116-ℓ, m, ρ, $\dot{\rho}$ Corrector for Ionospheric Refraction, GSFC Internal Memorandum, Nov. 1965.

7. Parker, H. C., Refraction Correction Intercomparison, Proc. of the GEOS Program Review Meeting, Vol. III, Tracking Intercomparison Tests with GEOS-I, GSFC, Dec. 1967.

8. Garriott, O. K., F. L. Smith, III, and P. C. Yuen, Observations of Ionospheric Electron Content Using a Geostationary Satellite, Planet, Space Sci., 13, 829-838, Aug. 1965.

9. Thomas, T. O., "The Electron Density Distribution in the F-Region of the Ionosphere," Electron Density Profiles in the Ionosphere and Exosphere, Ed. B. Maehlum, MacMillan Co., 1962.

10. Ratcliffe, J. A., and K. Weekes, "The Ionosphere," Physics of the Upper Atmosphere, Ed. J. A. Ratcliffe, Academic Press, 1960.

11. Risbeth, H., A Review of Ionospheric F-Region Theory, Proc. IEEE, 55, No. 1, pp. 16-35, Jan. 1967.

12. Gooding, R. H., Orbit Determination from Minitrack Observations, Roy. Soc. of London, A, 262, 79-88, 1967.

13. Berbert, J. H., J. D. Oosterhout, P. D. Engels, and E. J. Habib, Minitrack Calibration System, Photo. Sci. & Eng., 7, 77-83, Mar. and Apr. 1963.

14. Al'pert, Ya. L., On the Refraction and Doppler Shift of Radiowaves Radiated by AES in a Three Dimensional Heterogeneous Ionosphere, (English Trans.), Geomagnetism and Aeronomy, 3, 505-511, 1963.

15. Mityakova, N. A., and E. Yc. Mityakova, A Method for Investigation of the Ionssphere by the Ground Reception of Radio Signals from Artificial Earth Satellite, (English Trans.) Geomagnetism and Aeronomy, 3, 694-701, 1963.

16. Freeman, J. J., Final Report, NASA Contract No. NAS 5-3574, Oct. 15, 1964.

17. Yeh, K. C. and B. J. Flaherty, Ionospheric Electron Content at Temperature Latitudes During the Declining Phase of the Sunspot Cycle, J. G. R., 71, 4557-4570, 1966.

18. Ionospheric Predictions, Inst. of Telecommunication and Aeronomy, ESSA, Aug. 1966.

19. Al'pert, Ya. L., Investigation of the Ionosphere and of the Interplanetary Gas with the Aid of Artificial Satellites and Space Rockets, Sov. Phys. – Uspeki, 3, 479-503, 1961 (English Trans.)

20. Wright, J. W,, "Diurnal and Seasonal Changes in Structure of the Mid-Latitude Quiet Ionosphere," J. of Res. (NBS)-D, Rad. Prop., 66D, 297-312, 1962.

21. Chan, K. L., On the Topside Ionosphere over the American Continent, Rad. Sci., 1 (New Series), 1158-1162, 1966.

22. Kelso, J. M., "Radio Ray Propagation in the Ionosphere," McGraw-Hill Book Co., New York, 1964.

23. Browne, I. C., J. V. Evans, J. K. Hargreaves, and W. A. S. Murray, "Radio Echoes from the Moon," Proc. Phys. Soc. (London) Ser. B, 69, 901-920, 1956.

24. Bauer, S. J. and F. B. Daniels, Measurements of Ionospheric Electron Content by the Lunar Radio Technique, J. G. R., 64, 1371-1376, 1959.

25. Titheridge, J. E., Large-Scale Irregularities in the Ionosphere, J. G. R., 68, 3399-3417, 1963.

26. Olatunji, E. O., The Total Columnar Electron Content of the Equatorial Ionosphere, JATP, 29, 277-285, 1967.

27. Tyagi, T. R., Satellite Beacon Studies of the Ionosphere over Delhi, Sci. Rept. 34, National Physical Lab., Delhi, India, Aug. 1, 1967.

28. Rufenach, G. L., V. T. Nimit, and R. E. Leo, Faraday Rotation Measurements of Electron Content near the Magnetic Equator, J. G. R., 73, 2459-2468, 1968.

29. Basu, S., and A. Das Gupta, Latitude Variation of Electron Content in the Equatorial Region under Magnetically Quiet and Active Conditions, J. G. R., 73, 5599-5602, 1968.

30. de Mendonca, F., "Ionospheric Electron Content and Variations Measured by Doppler Shifts in Satellite Transmissions, J. G. R., 67, 2315-2337, 1962.

31. Bertin, F. J., Papet-Lepine, E. Vassy, Geographical Distribution of Total Electron Content Dependence on Geomagnetic Activity, Rad. Sci., 1, (New Ser.), 1131-1134, 1966.

32. Weise, A. P. and K. C. Yeh, Latitude Dependence of Ionospheric Electron Content, Tech. Rept., Elec. Eng. Res. Lab., Univ. of Illinois, 1967.

33. Rai, D. B., and J. L. Hook, Total Electron Content and Its Variations in the Auroral-Zone Ionosphere During Winter, JGR, 72, 5319-5324, 1967.

34. Liszka, L., Latitudinal and Diurnal Variations of Ionospheric Electron Content near the Auroral Zone in Winter, Radio Sci (New Ser.), 1, 1135-1966.

35. Merrill, R. G., R. S. Lawrence, and N. J. Roper, Synoptic Variations and Vertical Profiles of Large-Scale Ionospheric Irregularities, J. G. R., 68, 5463-5459, 1963.

36. Lawrence, R. S., D. Posakony, O. K. Garriott, and S. C. Hall, Measurements of the Total Electron Content of the Ionosphere at Middle Latitude near the Peak of the Solar Cycle," J. G. R., 68, 1889-1898, 1963.

37. Roger, R. S., Measurements of Large Scale Irregularities in the Total Electron Content of the Daytime Ionosphere, JATP, 26, 499-508, 1964.

38. Bhonsle, R. V., A. V. da Rosa, and O. K. Garriott, Measurements of the Total Electron Content and the Equivalent Slab Thickness of the Midlatitude Ionosphere, Rad. Sci., J. of Res., 69D, 929-937, 1965.

39. Vonbun, F. O., Power Requirements for the New 136 Mc Minitrack System, Internal Memo, GSFC, Sept. 1, 1960.

40. Wright, J. W., A Model of the F-Region Above h_{max} F2, J. G. R., 65, 185-191, 1960.

41. Grenchik, T. J., and B. H. Putney, A Review of Goddard Range and Range Rate System Measurements and Data Processing Techniques, GSFC, X-551-69-137, Apr. 1969.